1989

Electron beam decompositions of ionic crystals

Qun Dou
Iowa State University

INFORMATION TO USERS

The most advanced technology has been used to photograph and reproduce this manuscript from the microfilm master. UMI films the text directly from the original or copy submitted. Thus, some thesis and dissertation copies are in typewriter face, while others may be from any type of computer printer.

The quality of this reproduction is dependent upon the quality of the copy submitted. Broken or indistinct print, colored or poor quality illustrations and photographs, print bleedthrough, substandard margins, and improper alignment can adversely affect reproduction.

In the unlikely event that the author did not send UMI a complete manuscript and there are missing pages, these will be noted. Also, if unauthorized copyright material had to be removed, a note will indicate the deletion.

Oversize materials (e.g., maps, drawings, charts) are reproduced by sectioning the original, beginning at the upper left-hand corner and continuing from left to right in equal sections with small overlaps. Each original is also photographed in one exposure and is included in reduced form at the back of the book. These are also available as one exposure on a standard 35mm slide or as a 17" x 23" black and white photographic print for an additional charge.

Photographs included in the original manuscript have been reproduced xerographically in this copy. Higher quality 6" x 9" black and white photographic prints are available for any photographs or illustrations appearing in this copy for an additional charge. Contact UMI directly to order.

U·M·I

University Microfilms International
A Bell & Howell Information Company
300 North Zeeb Road, Ann Arbor, MI 48106-1346 USA
313/761-4700 800/521-0600

Order Number 9014893

Electron beam decompositions of ionic crystals

Dou, Qun, Ph.D.

Iowa State University, 1989

U·M·I
300 N. Zeeb Rd.
Ann Arbor, MI 48106

Electron beam decompositions of ionic crystals

by

Qun Dou

A Dissertation Submitted to the
Graduate Faculty in Partial Fulfillment of the
Requirements for the Degree of
DOCTOR OF PHILOSOPHY

Department: Physics
Major: Solid State Physics

Approved:

Signature was redacted for privacy.

In Charge of Major Work

Signature was redacted for privacy.

For the Major Department

Signature was redacted for privacy.

For the Graduate College

Iowa State University
Ames, Iowa

1989

TABLE OF CONTENTS

INTRODUCTION

When a solid is irradiated by ultraviolet or X-ray photons or electrons with similar energy (from a few electron volts (eV) to thousands of eV), electrons in the solid can be excited into higher energy states by absorbing either part (electrons) or all (photons) of the energies of the incoming particles. The excited state electrons can de-excite several ways, either by emitting a photon, giving rise to luminescence, or they may deexcite nonradiatively. The possible nonradiative processes are:

1. Transfer of electronic energy to vibrational energy, generating heat. This is usually the case for valence electron excitation.
2. Transfer of electronic energy to other electronic processes, such as Auger processes, photoemission, and secondary electron emissions from these processes. This often happens with core-level excitations.
3. While the electrons are in the excited state, the interactions between the atoms in the solid can be changed from bonding to anti-bonding. Thus the electronic energy can be changed to kinetic energy of the atoms or ions, causing changes in configuration, that is, forming defects and inducing decomposition of the solid.

Processes 1 and 2 are observed in all solids. Process 3, however, is efficient only in insulators. This is because in metals or semiconductors the lifetimes of the excited states are usually very short ($< 10^{-15}$ seconds), due to the existence of free electrons. A longer lifetime of the anti-bonding state is needed for the formation of

defects. For example, one can estimate that for a sodium atom, with 10 eV of kinetic energy, approximately 10^{-12} second will be needed to move one atomic spacing, about 4 Å). In insulators the lifetimes of the excited states are much longer, allowing higher efficiency for process 3.

The problem addressed in this dissertation is intimately related with process 3 listed above. In 1967, Palmberg and Rhodin [1] and Townsend and Kelly [2] first observed the desorption of alkali and halogen atoms and ions from alkali halides causing decomposition of the crystals and change in stoichiometries of their surfaces by low energy electron radiation. Later it was shown that photons with similar energy can produce the same effect. In the following years, this phenomenon was studied in great detail. However, although an enormous amount of experimental and theoretical work has been done on this system, new phenomena continues to be discovered and a detailed mechanism of the electron beam decomposition of alkali halides is still lacking [3, 4]. In this study, we investigated electron interaction with alkali halides in searching of the mechanism governing the process of electron beam decomposition. It is also our intention to determine if the phenomenon of desorption from ionic crystals can be used as a new surface spectroscopy. Another insulator that is closely related to alkali halides, CaF_2, was also studied.

The formation and breaking of chemical bonds is central to many aspects of modern physics and chemistry. Through studies of low energy electron beam interaction with insulators one can gain information on this important basic problem of the energy transfer and bond breaking in

solids. There is a practical aspect to this study as well. Much of our understanding of solids, and especially of their surfaces, comes from studies of electron and photon beam interactions with solids, such as low energy electron diffraction (LEED), electron energy loss spectroscopy (EELS), Auger spectroscopy, and photoemission, all involving radiation of energies from several eV to a few keV. Numerous examples exist that show these probing beams actually change the systems being studied [5], either due to stimulated desorption or enhanced diffusion. It has also been reported that electron irradiation can cause changes in surface geometry and composition in several materials [6, 7]. So it is also of practical importance that we have a good understanding of, and be able to characterize the effects of these radiations.

Alkali Halides And Radiation Induced Defects

Alkali halides are often taken as prototypes of ionic crystals and insulators, and their physical properties are considered to be well understood.

Alkali halides are, as the term ionic crystal implies, made up of positive alkali ions and negative halogen ions. The ionic bond results from the electrostatic interaction between these ions. Most alkali halides have the so called sodium chloride structure, in which equal number of alkali and halogen ions are placed at alternative points of a simple cubic lattice, with each ion having six ions of opposite charge as nearest neighbors (Fig. 1). CsCl, CsBr and CsI are the exceptions. They have the cesium chloride structure, which consists of equal number of Cs

and halogen ions at the points of a body-centered cubic lattice so that each ion has eight of the other kind as nearest neighbor. In this study, we are restricted to only sodium chloride structured alkali halides.

It has long been known that electron and photon irradiation can create defects in ionic crystals. The study of defects and radiation induced defect creation processes in alkali halides dates back to the beginning of this century. The defects produced are point defects, i.e., they are localized to a few atomic spacings. Most of them are in the halogen sublattice. Alkali defects can be produced by collision with high energy ions but not electrons or photons. They consist of equal number of vacancies and interstitials, which are called Frenkel pairs. Because these defects give rise to optical absorption (coloring) in a normally transparent region, they are also called color centers. The color centers are categorized according to the positions of their absorption peaks. There is a large number of these with different structures. A list of some of them is given in Table 1.

Of the many mechanisms proposed to explain the process of radiation induced defects, the one offered independently by Pooley [8, 9] and Hersh [10] for the production of F centers (a halogen vacancy with a bound electron) and H centers (a singly ionized di-halogen molecule occupying a halogen site) gained the most support and acceptance. The model was based on the observation that the temperature dependence of F center production rate and luminescence anticorrelate in the temperature range between 50 to 200 K. It was proposed that the initial excitation that leads to the formation of defects is an exciton, as opposed to ionization

Figure 1. Crystal structure of alkali halides (sodium chloride type).

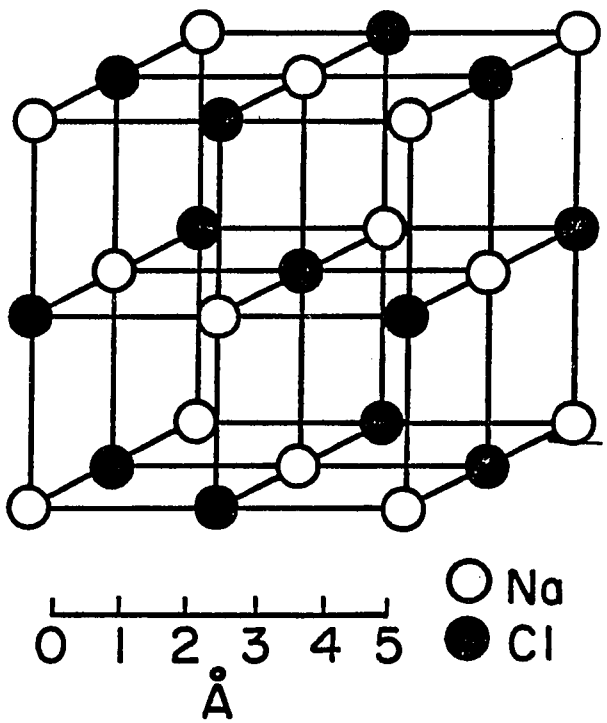
Na
Cl
0 1 2 3 4 5
Å

Table 1. A list of some color centers in alkali halides

F center	an electron bound to a halogen vacancy
H center	a singly ionized halogen molecule (X_2^- occupying a halogen site.
V_k Center	a X_2^- ion located on adjacent halogen sites, with bond direction along (110).
Aggregates	two, three or four F centers can become nearest neighbors through diffusion, forming M, R and N centers

processes. An exciton is simply a spatially correlated electron-hole pair, an electronicexcited state. Because of this space correlation, the exciton states have lower energies than the conduction band, and manifest themselves in optical absorption spectra as peaks just below the lowest interband transition. In an alkali halide an exciton can cause deformation in the lattice, which results in the holes becoming localized, or being trapped by a pair of halogen ions along the (110) direction. Such a configuration is called a self-trapped-exciton(STE). The luminescence radiation that anti-correlates with the F center production rate was identified to be from the de-excitation of the lowest triplet state of the STE (pi polarized STE) [11, 12, 13]. When the STE de-excite non-radiatively, the electronic energy is transformed into kinetic energy, resulting in an electron occupying a halogen vacancy site and a closely spaced halogen atom interstitial, an F-H pair. This pair is further separated by the H center's motion along a (110) row through a collision sequence.

The temperature dependence of the relative intensity of the radiative and non-radiative processes can be explained by using a configuration coordinate diagram (Fig. 2) [14]. Under the Frank-Condon approximation, the electronic transition occurs without changing the distance between the ions. This is shown in Fig. 2 as the process between ground state equilibrium point A to an excited state point B with the same configuration. Then the nucleus would move to a new equilibrium point X_c. The system can go through a de-excitation process (C-D) by emitting a photon, giving rise to luminescence. However, if the

temperature is high enough to offer the activation energy U, so that the ground state and the excited state have the same configuration, then it is also possible for the system to go through a radiationless transition and convert the electronic energy to kinetic energy of the nucleus. Thus higher temperature favors defect creation and decreases luminescence. This effect is known as thermal quenching.

Some other proposed mechanisms for defect creation involve ionization processes. Double ionization of a halogen ion [15] or single ionization of two adjacent halogen ions [16, 17] can result in a halogen ion in a repulsive potential, and this can lead to the formation of defects. These processes are less efficient than the excitonic process because of the smaller cross section of the ionization process. But it is possible that these processes play a secondary role in defect creation [18, 19]. Numerous studies using pulsed electron and photon beams have shown that the initial defects produced are F and H centers at all temperatures [20, 21, 22, 23]. F centers are formed in about 11 picoseconds while H centers develop within a few nanoseconds. At liquid helium temperature, the F and H centers are the only products. At higher temperatures, the F and H centers become mobile and will undergo various reactions to form new defects. Thus the Pooley-Hersh mechanism is believed to be the fundamental one for the defect production process in alkali halides.

It has also long been known that F Centers in alkali halides can form dimers, trimers and even larger clusters through a diffusion process. This results in the formation of an alkali metal rich region.

Figure 2. Configuration coordinate diagram for excitation and radiative deexcitation and non-radiative deexcitation.

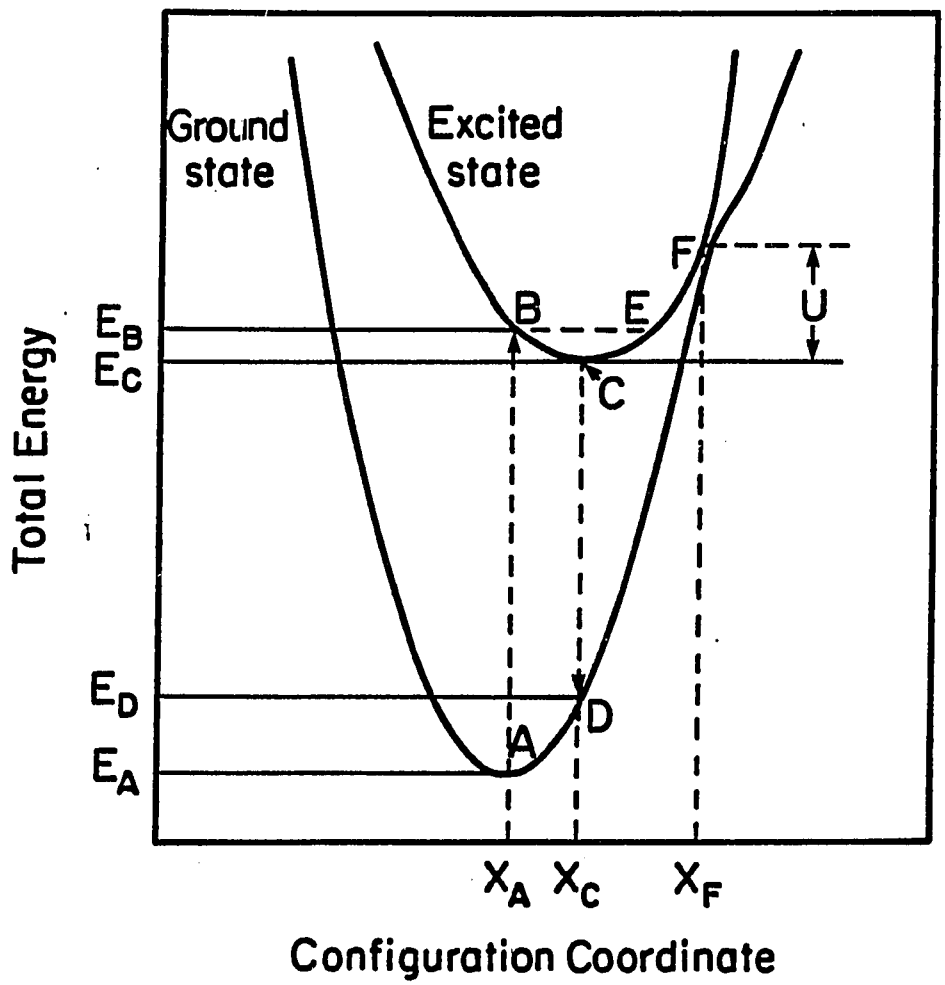
Ground state
Excited state
F
B
E
U
E_B
E_C
C
E_D
D
A
E_A
X_A X_C X_F
Total Energy
Configuration Coordinate

When annealed at moderately high temperatures (200°C for NaCl), metal clusters, known as colloids, of sizes up to a micrometer, can be formed [24, 25, 26, 27]. As we will show later, these colloids play an important role in the desorption process.

Electron-Stimulated Desorption From Alkali Halides

The first observation of electron-stimulated desorption was made on gas adsorbate systems in early 1960s [28, 29]. This excited great interest and the phenomenon was studied extensively in the following years. Typical systems studied include hydrogen, oxygen, carbon monoxide and carbon dioxide adsorbed on various transition metal surfaces. It was observed that the irradiation of solid surfaces containing gas adsorbates with low energy electrons can cause the desorption of atoms, molecules and ions of the gases that were adsorbed on the solid. The desorption yield is linearly proportional to the bombarding electron current and is of the order of 10^{-3} to 10^{-8} per incident electron. This translates to a cross section of about 10^{-18} to 10^{-23} cm^2 (compared to 10^{-16} cm^2 for gas phase decomposition). Neutral atoms are the most abundant of the desorbed species, but for experimental reasons most studies concentrated on ion desorption. The electron energy dependence of the yields show significant onsets at core-levels of the adsorbate [30, 31, 32]. It was also observed that the ions tend to desorb in discrete cones in directions determined by the orientations of the bonds that were broken by the desorption process. This effect, sometimes called electron-

stimulated-desorption-ion-angular-distribution (ESDIAD), in turn, has been used to study the structure of the gas molecule adsorption on the surfaces [33, 34].

After the initial observation of electron beam induced decomposition of alkali halides [1, 2] the phenomenon has been studied under several names: sputtering, desorption induced by electronic transitions (DIET) and electron- or photon- stimulated desorption (ESD,PSD). We will use the term ESD in the following discussions (all studies show that electrons and photons have similar effects). Through many years of experimental work it has been shown that:

A) The products of ESD include positive ions and neutral atoms of alkali and halide. Some of the desorbed alkali atoms are in excited states [35, 36]. There are also small amounts of diatomic halide molecules. Of all the desorbed species the ground state neutrals are dominant, with a yield about 1 to 10 per incident electron, which is much bigger than the desorption yields from gas adsorbates [37]. There is evidence that the excited state alkalis may be due to the desorbed ground state neutrals which were excited by secondary-electrons [38]. The ions among the desorbed species may also come from neutrals ionized by secondary electrons [39].

B) Stoffel et al. [40] studied the dependence of the ground state Na neutral atom desorption yield on incident energy on a series of sodium halides. The yields were shown to increase with increasing energy, reaching a maximum at about 100 eV, and then decrease at higher energies, possibly due to the increased depth of penetration. Onsets were observed

at the Na 2p exciton energies of the respective halides (41-46 eV). The structures are similar to those of soft x-ray absorption spectra. The work of Parks et al. [41], also showed the same resemblance at the Na 1s region. This raised the hope that the ESD from alkali halides can be used as a spectroscopy to study the bonding energies. This technique would be intrinsically surface sensitive. However, it is not clear whether these structures at metal core levels indicate any core-hole related processes or just reflect the increased absorption.

There were few detailed threshold measurements. Haglund et al. [42] showed that the ground state neutral Na desorption from NaCl did not feature a clear cut threshold, while the initial onset was about 20 eV. Pian et al. [43] and Yasue and Ichimiya [44] measured the threshold of excited-state Na and positive Li ion desorption from NaCl and LiF respectively. In each case, the threshold energies were smaller than the core-exciton energies (65 eV for Li 1s in LiF), so the core excitation is not a necessity for ESD.

C) Measurements of the kinetic energy distribution showed that the energies of desorbed alkalis always obey a Maxwellian distribution, given by

$$N(E) = C\, E^{1/2}\, \mathrm{EXP}(-E/kT) \qquad (1)$$

where E is the kinetic energy, k is the Boltzmann constant and T is the temperature [45, 46]. The fitted temperature is very close to that of the sample. The halogen energy distributions are more complicated. The

work of Overeijnder et al. showed that at temperatures above 200°C, the halogen energy distribution followed (1). Below 150°C, however, a non-thermal distribution (a high energy tail with cutoff energy as high as 1.34 eV) occurred in some alkali halides, while the distribution remained thermal in others. The difference between these two groups seems to be that the ones with non-thermal distributions have their lattice parameter satisfy

$$s/d > 0.33$$

where s is the distance between two halogen ions and d is the diameter of a halogen atom. This observation, together with the theory of Townsend [47] that H centers can only occur in those systems with $s/d > 1/3$, suggests that the high energy halogens originated from H center migration. The kinetic energies of halogen molecules were shown to follow (1) at all temperatures [48], indicating that they are formed by combining two halogen atoms at the surface, which then evaporate. The halogens with non-thermal energies do not participate in this process.

D). Townsend and his co-workers studied the angular distribution of ESD from (100) surfaces of single crystal samples. They showed that the non-thermal halogens are emitted directionally, while alkalis and thermal halogens are not [49]. Their result showed that the non-thermal halogen yields were peaked at directions that correspond to (110) and (112) crystallographic directions, and this was believed to be caused by focused collisions along the close-packed directions. This, however,

disagrees with a more recent experiment by Postawa and Szymonski [50], which showed that the non-thermal yield actually peaked at the normal direction to the surface.

E). By using a chopping technique, Overeijnder et al. [51] showed that the delay times for nonthermal halogen desorption were smaller than 10-4 s (the instrumental resolution). The thermal halogen and alkalis were shown to have a small portion that does not desorb immediately. The delay time is about 0.5-1.0 ms. This delay time is independent of temperature, thus it can not be due to migration of defects to the surface. Overeijnder et al. suggested that this was due to the lifetime of the excited state. Similar results were obtained by Kanzaki and Mori [52]. Loubriel et al. [53, 54] found that at high temperatures (above 600 K in LiF), the ground state desorption persists for seconds after the electron beam is turned off. They attributed this effect to the slow diffusion of F centers. By measuring the temperature dependence of this effect, the derived an activation energy of 0.7 eV for the assumed F center diffusion.

F). Numerous studies [55, 56, 57, 58, 59] have shown that electron irradiation causes changes in surface stoichiometry and produces a alkali metal rich layer on the surface of alkali halides. The new composition is dependent on both the electron intensity and the sample temperature.

Mechanisms Of Desorption

When a solid is irradiated by a beam of particles, energy can be transferred either by a classical two-body collision or by electronic

excitations. In the case of particle-particle collisions, the maximum amount of energy that can be transferred is given by

$$Emax = 4\ M\ mE\ /\ (M+m)^2$$

where M and m are the masses of the two particles and E is the incident kinetic energy. It is easy to show that in the case of an electron beam, due to the small electronic mass, energy transferred this way would be too small to cause any damage. So it is electronic excitation by the electrons and photons that leads to the desorption and the decomposition of the ionic crystals.

The ESD from gas adsorbate systems can be understood qualitatively by the model of Gomer-Menzel-Redhead (GMR) [28, 29]. It is proposed that the electron irradiation causes a Frank-Condon transition from the ground state to one of the excited states. After the excitation, the gas ion is in a repulsive state and starts to move away from the surface. Most of the ions will return to the ground state before leaving the surface through an electron tunneling process due to their proximity to the surface. This accounts for the smaller ESD cross section compared to the gas phase decomposition.

The case of ESD from alkali halides is much less clear. Many mechanisms have been proposed to explain the desorption effects from alkali halides. These mechanisms can be divided into two categories: direct and indirect. In a direct mechanism, which is similar in spirit with the GMR model, the primary electrons or photons cause the change

from a bonding state to an anti-bonding state at or near a surface site. For example, Varley [15] suggested that double ionization of a halogen negative ion could lead to the creation of defects. Similar processes near the surface can lead to the desorption of halogen and alkali positive ions. A similar approach was taken by Knotek and Feibelman (KF) [60, 61, 62, 63]. They proposed that in a maximum-valence ionic material, following the creation of a core-hole on an alkali ion, an inter-atomic Auger process can occur with large magnitude (due to the lack of valence electrons on an alkali ion). This inter-atomic Auger process will fill the hole on the alkali ion and at the same time eject another electron from the halogen site, thus making it a positive ion. The KF mechanism was supported by ion desorption data from materials like TiO_2 and WO_3, mainly through threshold measurements.

The indirect mechanisms recognize the fact that electrons and photons can penetrate deeply into the crystal, and deposit a large amount of energy in the bulk, which then leads to generation of localized defects.

Based on the model of Pooley and Hersh [8, 9, 10] on defect creation, Szymonsky [64], and Agullo-Lopez and Townsend [65] proposed that the desorption process started with the creation of F-H pairs via the generation of self-trapped excitons. The pair will then separate to produce stable F and H centers. The H centers can migrate along the <110> directions of the crystal through a replacement collision sequence. When such an H center reaches the surface, it releases a halogen atom with non-thermal energy. Or the H center can diffuse randomly and when

reaching the surface release a thermal halogen. Thermal evaporation of the alkali metal particles left on the surface is assumed to be responsible for their desorption.

Currently the indirect mechanism is considered the preferred one. The direct mechanisms for ESD from alkali halides face several difficulties. There is doubt whether the repulsive states produced by electronic excitation can live long enough in alkali halides, since the relaxation of the lattice after the charge reversal can prevent the desorption from happening [66]. It can not explain the huge cross section derived from the yield assuming only a surface process. To explain the dominance of the neutrals among the desorbed species, one has to assume a process of electron capturing (neutralization) which is not supported by direct experimental observations.

When the work in this thesis started in 1984, the picture was less clear. Much attention was focused on the excited state neutral and ion desorptions. It was incorrectly believed that the desorbed excited state neutrals consist of only those in their first excited state, thus implying the exisistence of a selection rule and a direct process. It was not until 1986 [38, 39] when Walkup et al. published their work that it was understood that all excited states are represented in the desorbed species, and the ground state desorption is the primary process while the excited state neutral and ion desorptions are secondary processes. As a result, the indirect mechanism became more reasonable.

EXPERIMENTAL

The schematic diagram of the experimental setup is shown in Fig. 3. The electron gun was built after the design of Erdman and Zipf [67, 68]. It consists of a tungsten filament, a five-element electron lens system and two pairs of deflecting plates. The electron beam has a diameter of 1mm and a current up to 10 μA. The base pressure of the chamber is about 5×10^{-10} Torr and is below 1×10^{-9} Torr during the experiment. A Spectro Scientific SM1000 residual gas analyzer (RGA) was used to detect the desorbed species. Since the halogen gases tend to build up in the chamber, thus giving a large, unstable background for the halogen signals, we used modulation techniques to enhance the signal-to-noise ratio. The electron beam was modulated at a frequency of 20 Hz by applying a square wave voltage to a pair of deflecting plates, while the output of the RGA was connected to a lock-in amplifier, using the modulation signal as reference. With this arrangement, the first harmonic output from the lock-in amplifier represents the intensity of the desorption, with negligible contribution from the background. This resulted in a greatly improved signal-to-noise ratio.

Excited-state neutral alkali atoms were detected by measuring the fluorescent photons emitted during de-excitation. The setup is similar to that of Tolk et al. [35]. A lens was placed near the window to collect the photons and focus them on the entrance slit of a monochromator, which was used to select the specific transitions. A photomultiplier cooled to -20°C, coupled with a

Figure 3. Schematic diagram of the experimental arrangement for studying ESD with mass-spectrometer and optical methods.

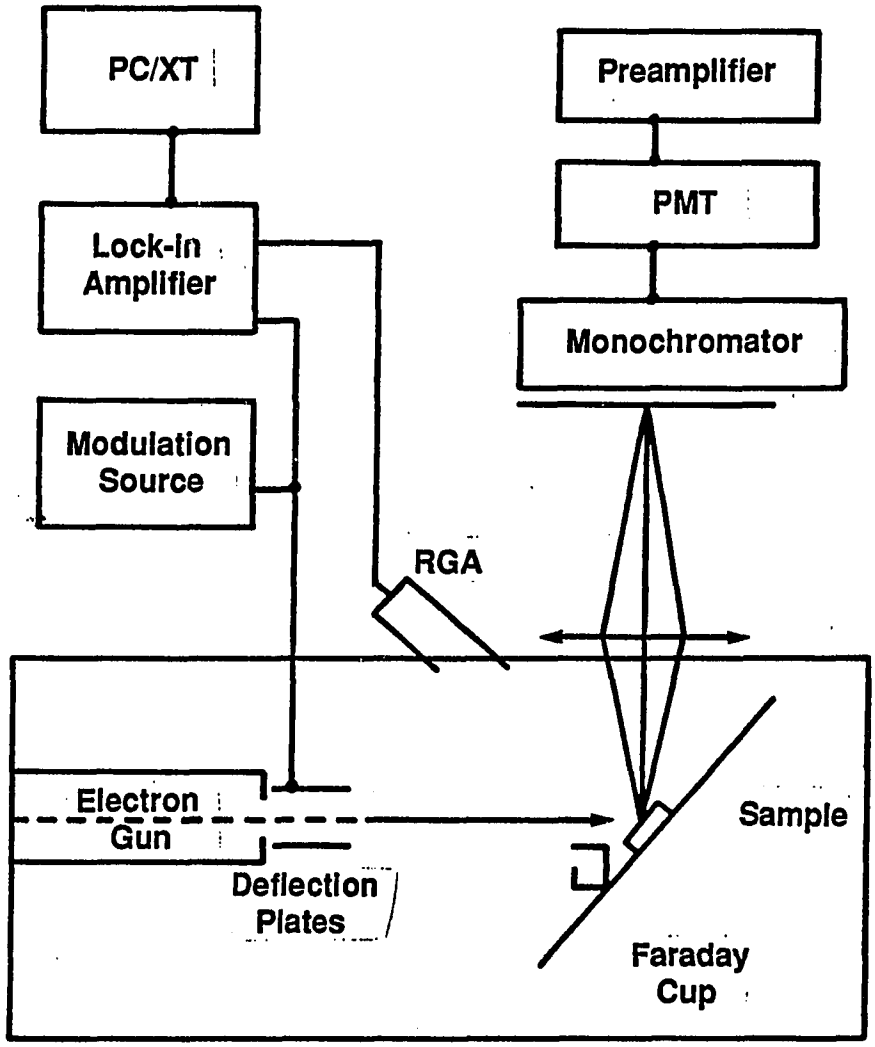
PC/XT
Preamplifier
PMT
Lock-in Amplifier
Monochromator
Modulation Source
RGA
Electron Gun
Deflection Plates
Sample
Faraday Cup

preamplifier/discriminator and a pulse counter, was used to measure the photon intensity. In this case, the background was mostly from the light emitted by the W filament of the electron gun, and it is also removed by modulating the electron beam.

When the electron beam was at the off-sample position, its intensity was measured by a Faraday cup connected to a digital ammeter, which is triggered by the negative slope edge of the modulating signal. The measured desorption yield is corrected for the electron current variations. The temperature of the sample can be varied from room temperature to 350°C by using a platinum wire heater. It was measured by a set of chromel-alumel thermocouples clamped onto the sample. The previous work of Tolk et al. [36] and Overeijnder et al. [46] showed that the temperature measured this way correlated with the surface temperature very well, and the effect of electron beam heating was negligible.

We found that the desorption signal decreased as a function of time, a phenomenon obviously related with the changes brought to the sample surface by the electron beam. To decrease errors in the temperature dependence measurements, we annealed the sample at 340°C for an hour before taking another measurement.

Our samples include commercial alkali halide single crystals from Harshaw and mixed KCl-NaCl crystal grown in our laboratory. The Harshaw crystals are known to contain some hydrides. The effect of these impurities on the desorption process is seldom addressed, although it could be an important factor due to the strong influence of impurities on defect formation [69]. However, since most other researchers in this

field also used Harshaw crystals, our results can be compared to theirs. The mixed KCl-NaCl crystal was grown in air from the melt. The eutectic composition (50 mole percent KCl) was used to ensure the homogeneity of the crystal. NaCl and KCl form a solid solution at all concentrations. All samples were cleaved in air before being put into the chamber, and repeatedly cleaned by baking at 350°C.

The scanning electron microscopy (SEM) and Auger spectroscopy experiments were done in a Perkin-Elmer 600 electron multiprobe system equipped with SEM, Auger spectroscopy, scanning Auger microscopy (SAM), and energy-dispersive x-ray emission spectroscopy. A highly focused ($d<2000$ Å) scanning electron beam, incident at 30° from the sample normal, was used both as the damaging source and the probe. The secondary electrons were collected by a collector held at a high positive voltage. The signal, together with the scanning voltage, was fed into a cathode-ray-tube (CRT) to form an image of the scanned area. A higher magnification can be achieved by scanning a smaller area. The contrast comes from both the topology and the composition of the surface, although the secondary electron emission is not very sensitive to the composition. The changes induced by the electron irradiation can be observed on the CRT in real time or can be recorded on a film by directing the signal to a camera. One can also choose to detect only those electrons with certain kinetic energies, at the energy of an Auger line of an element, for example, by using a cylindrical-mirror-analyzer. Subtracting the background signal obtained from one or two nearby points in the spectrum, such a scanning Auger micrograph gives the distribution of that element

in the scanned area.

Both thin film and single crystal samples were studied. The films were deposited on a Ni-coated silicon wafer by thermal evaporation, with thicknesses ranging from 500-4500 Å. The films were evaporated in a separate chamber at pressure lower than $5x10^{-8}$ Torr, while the crystals were cleaved in air before they were moved into the microscope. It has been reported that fresh alkali halide surfaces remain clean after exposure to air [70], and the Auger spectra we measured, which showed no trace of any contaminants, showed this to be so. The pressure in the working chamber was always lower than $5x10^{-10}$ Torr, and the samples usually remained free of contaminants throughout the experiments.

RESULTS AND DISCUSSION

Electron Radiation Induced Topological And Compositional Changes On Alkali Halide Surfaces

Of the many studies on ESD and PSD from alkali halides, most have concentrated on the emitted atoms and ions, in order to elucidate the mechanism. Few, if any, have commented on the surface itself. Few studies of ESD or PSD have recognized the possible importance of the highly damaged surface [71]. It is also known that in many desorption studies, macroscopic layers of material are lost from the surfaces [72], partly by evaporation at the elevated temperatures often used. In the following, we use scanning electron microscopy (SEM) and scanning Auger microscopy (SAM) to examine the morphology of surfaces undergoing desorption induced by an electron beam. Our results on thin films and single crystals show that considerable topological and compositional changes can occur on an alkali halide surface bombarded by electrons. These changes, we believe, should be taken into consideration when constructing a detailed mechanism for the ESD process.

Figure 4 shows the effect of electron beam irradiation on a LiF film. The rectangles are formed by rastering a well-focused electron beam on these areas for only a few seconds. At the center was a dust particle used for focusing. The electron beam energy was 5 keV and the sample was at room temperature.

In Fig. 5 are SEM pictures of LiF films. The sample was at room temperature. The topological changes of the film surface induced by

Figure 4. The effects of electron beam irradiation on a smooth LiF thin film. The dust particle in the center was used for focusing.

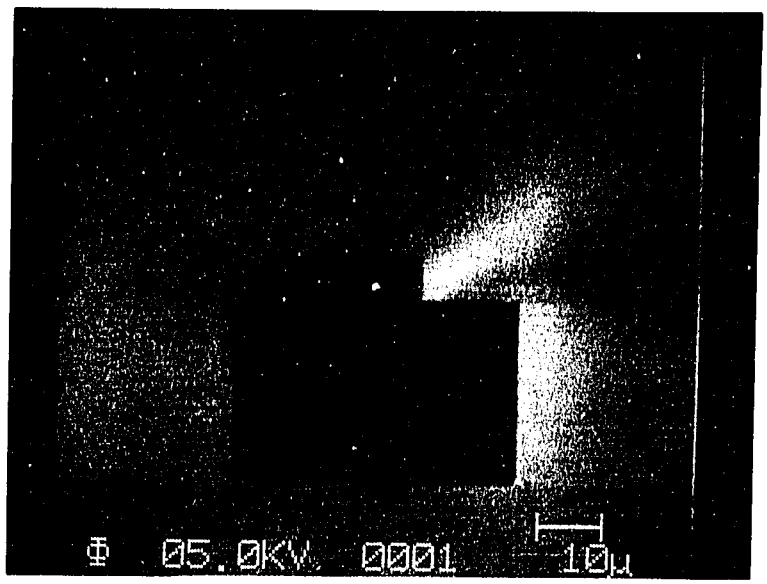
05.0KV 0001
10μ

Figure 5. SEM micrograph of LiF. A). 2000x. B). The lower-right corner of the central area in A. 5000x.

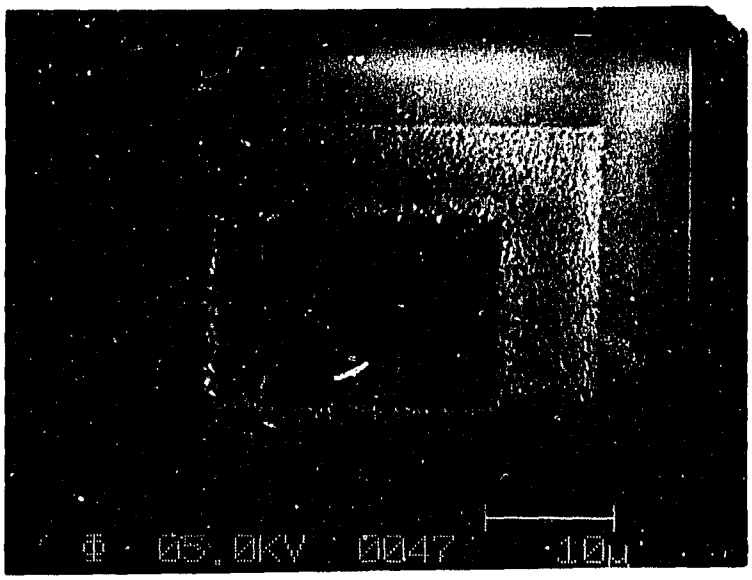
05.0KV 0047 10μ

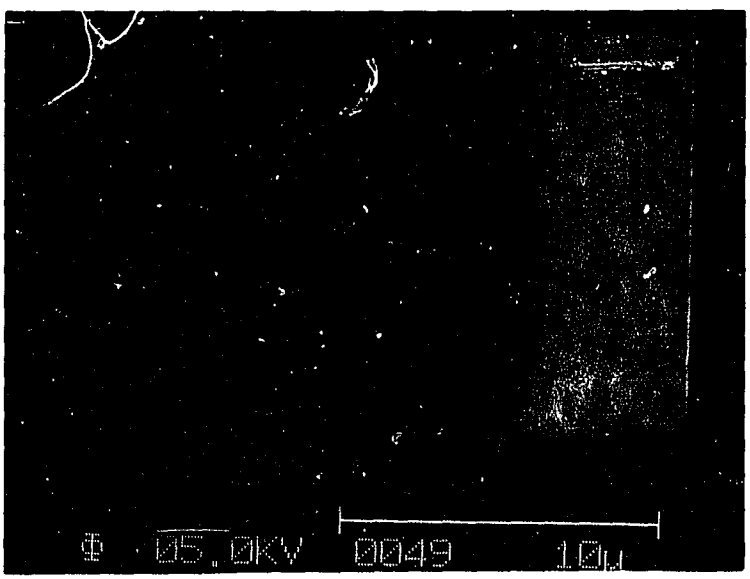
05.0KV 0049 10μ

electron irradiation can be seen clearly. The new structures, bright droplets as seen in the SEM, grew in size with radiation and eventually reached a steady state, with the biggest structures about 2 m in diameter. The three stages of damage shown in Fig. 5a resulted from the use of a different rastering size for the electron beam, with the center region having received the highest dose of radiation, approximately 25 mA/mm^2 X 10 min (10 nA of current focused to about 2000 Å). The outermost area had the least dose, and it shows the smooth surface of the LiF film before being damaged.

In Fig. 6 are SEM pictures of NaF and NaCl films at higher magnification. The experimental geometry is such that electrons hit the sample surface from the left-hand side of the picture, so the bright appearance of the left part of the spots shown in Fig. 6a means that the structure are bumps instead of depressions.

Figures 7 and 8 show SAM maps of the same areas. The alkali maps correlate with the bright spots in the SEM maps, indicating that these spots are metal rich. The fact that the halogen map anti-correlates with them rules out the possibility of only topological effects.

At elevated temperatures, the same topological changes could be observed (Fig. 9), but the droplets formed faster at higher temperatures so that it was difficult to obtain a scanning Auger micrograph.

The surfaces of these samples were free of contaminants within the detecting range of the AES (see Fig. 10), and they were kept clean throughout the experiment. We did find that after the samples have been irradiated by electron beams, they become gradually contaminated with

Figure 6. SEM micrographs. A). NaF at 5000x. B). NaCl at 7500x.

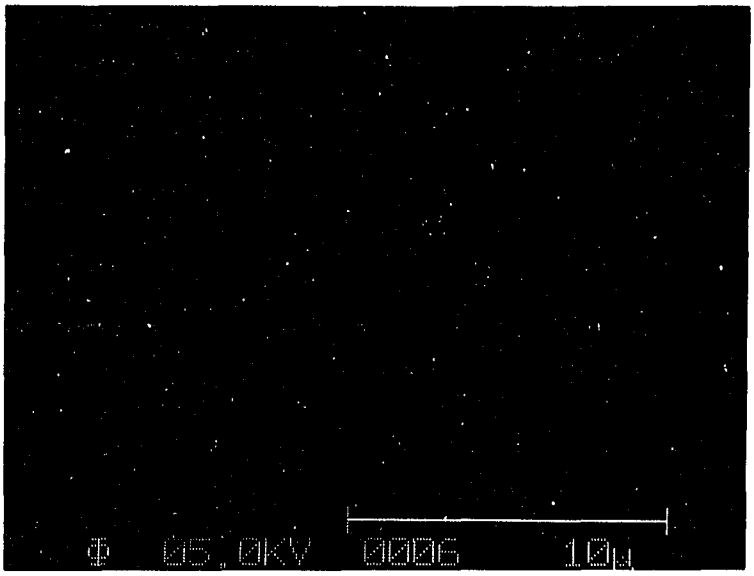
Φ 05.0KV 0006 10μ

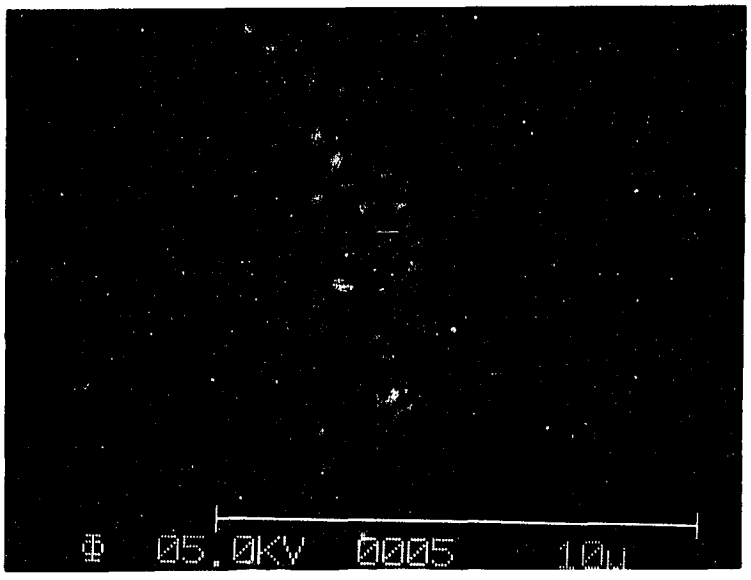
Φ 05.0KV 0005 10μ

Figure 7. SAM micrograph of LiF. Same area as in 5b. A). Li map of peak (50.0 eV) minus background (58 eV). B). F map. Peak/background = (658/679 eV)

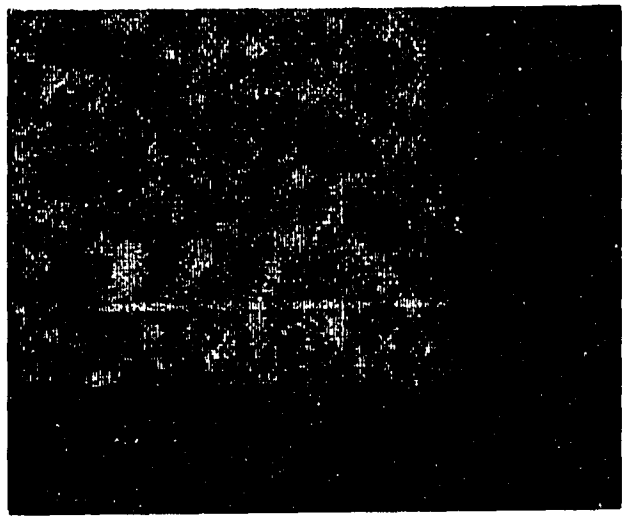

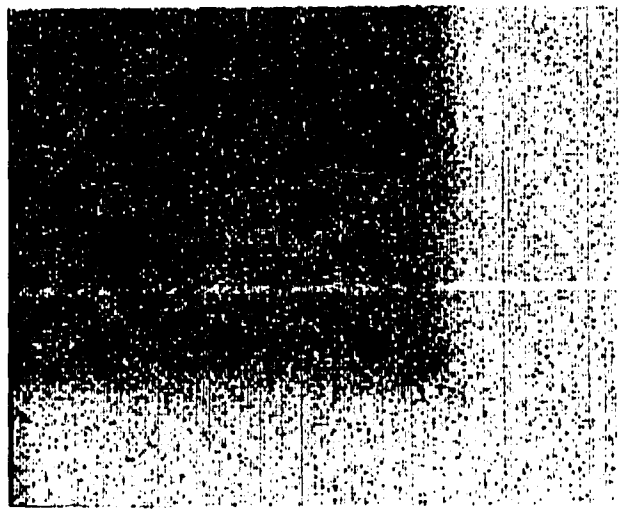

Figure 8. SAM micrograph of NaF. Same area as in 6a. A). F map with peak at 655 eV and background at 670 eV. B). Na map with peak

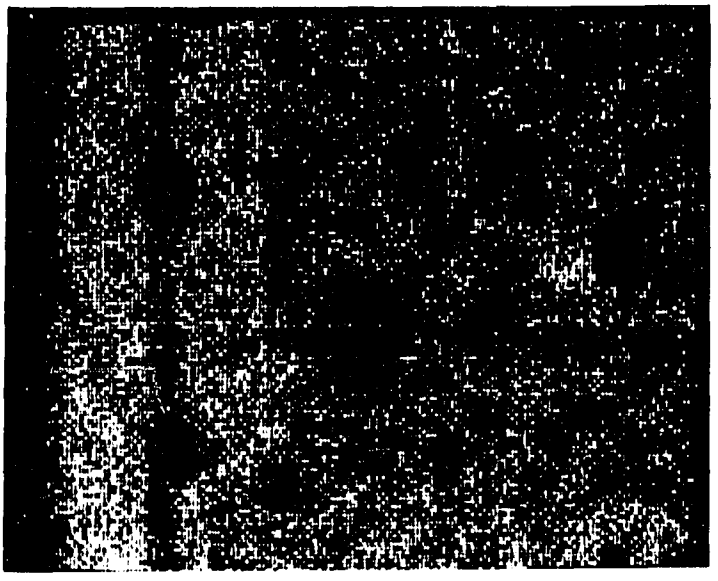

Figure 9. SEM micrographs. A). NaF at 90°C. B). LiF at 80°C.
at 994 eV and background at 1010 eV

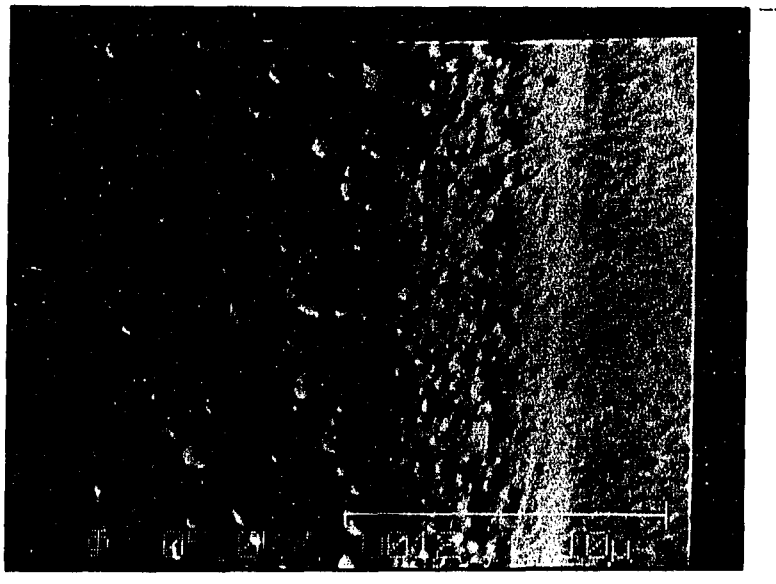

Figure 10. Auger spectrum of NaCl showing no trace of oxygen and carbon.

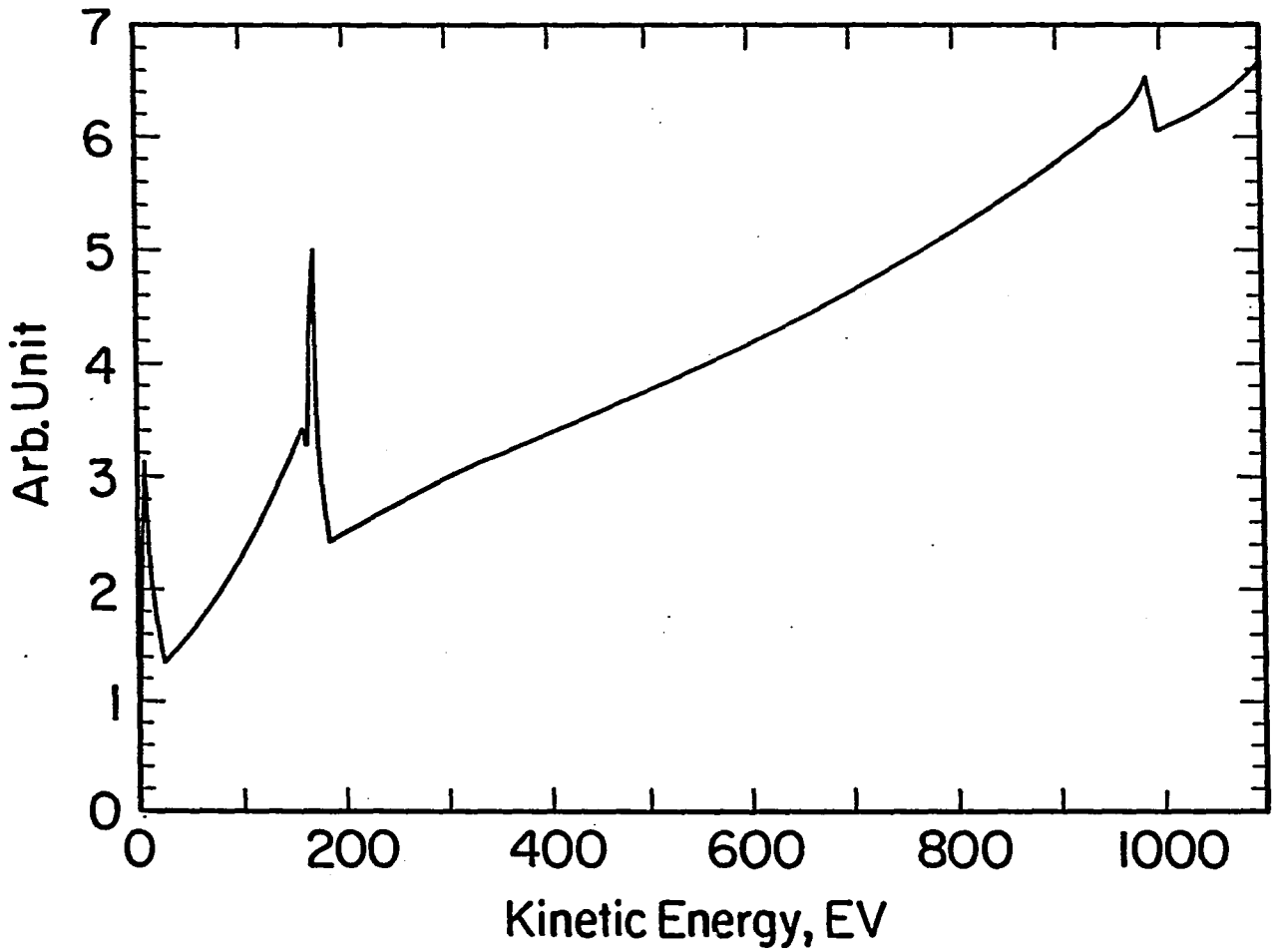
Arb.Unit
0
1
2
3
4
5
6
7
0
200
400
600
800
1000
Kinetic Energy, EV

oxygen and carbon, due to the oxidation of the free metal on the surfaces. On the other hand, we have used samples that were initially covered with carbon and oxygen, and observed identical topological changes. It is not possible to determine the alkali/halogen ratio in these structures, since focusing the electron beam on one of them would instantly change its composition. The instrument resolution, about 1000 Å, does not permit the observation of the detailed structures of these alkali metal clusters.

Similar electron-induced changes were observed on single crystal KCl (Fig. 11 and Fig. 12). The fact that the surface topology and composition were independent of whether a film or single crystal surface was studied indicates that the edges of the bumps are not correlated with grain boundaries in the films. It also shows that they are not oriented with respect to any crystallographic direction.

Elliot and Townsend [73] observed the formation of cones and pits on alkali halide surfaces by electron irradiation. They attributed this effect to the surface contaminants that did not desorb. However, the phenomena we observed can not be explained this way since: A) The structures can be formed on very clean surfaces; B) When the surface is covered by C and O_2, we still see similar structures.

These maps indicate that a new phase, rich in alkali metal, and possibly non-homogeneous, is formed on the surface as a result of electron irradiation. It is non-uniformly distributed on the surface, and clustered with sizes in the micron range. Since all previous experiments showed similarity between electron and photon irradiation-

Figure 11. SEM micrograph of a KCl single crystal. A). 7500x. B). Same area, 2500x.

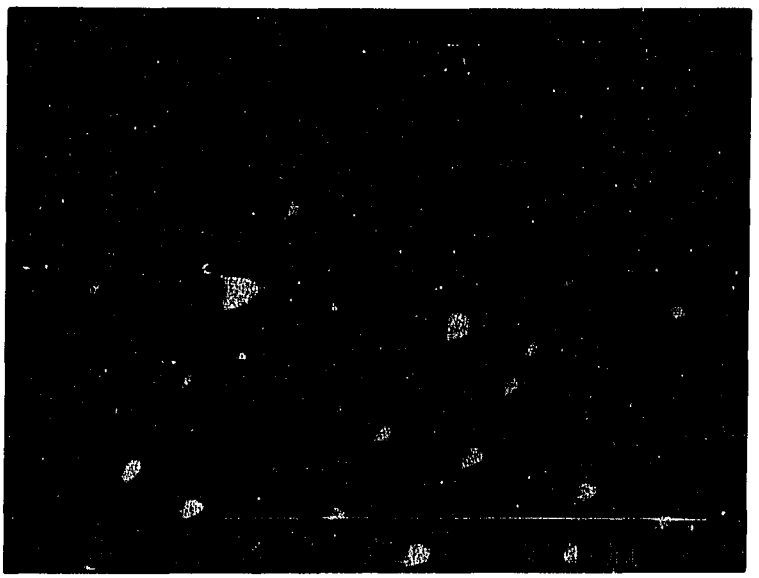

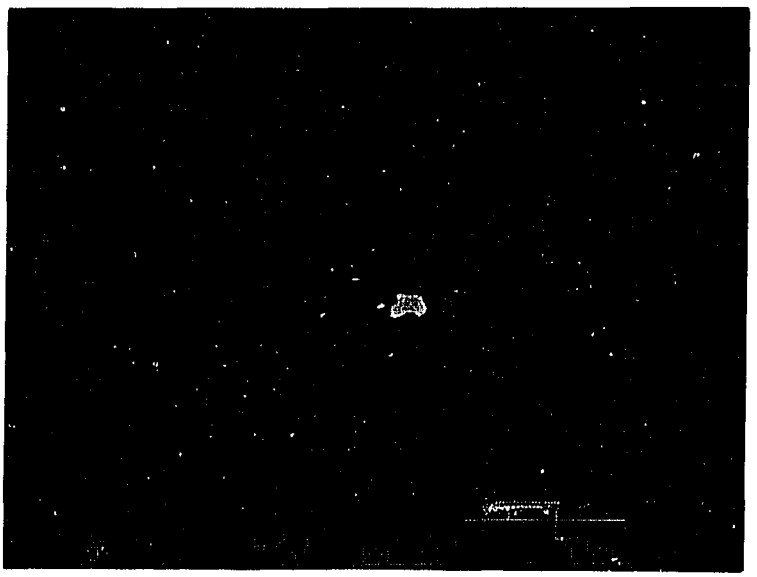

Figure 12. K^{+} SAM micrograph of a KCl single crystal.

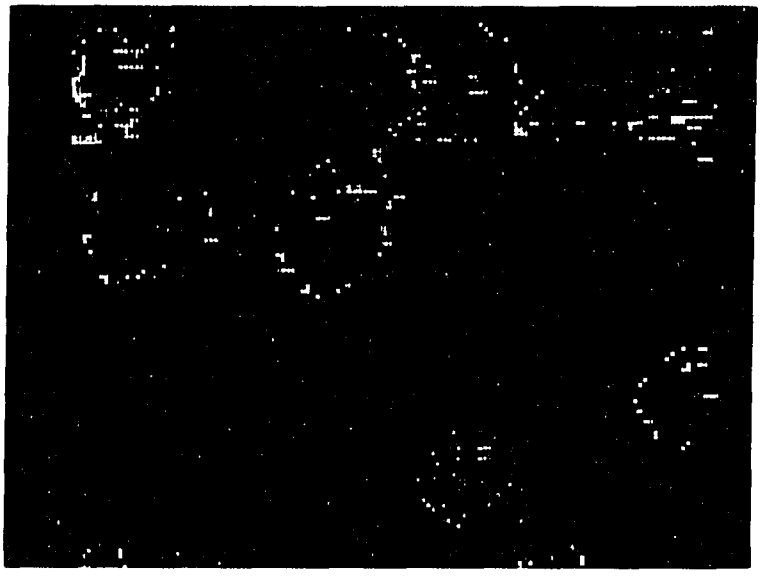

induced damage, we would expect that similar effects can be observed using photons. And indeed, such effects have been observed [74].

It has long been recognized that radiation can lead to the formation of colloidal alkali metal particles. These metal colloids, formed by additive coloring or x-ray radiation, were intensely studied as a bulk effect [26, 27]. Our data presented above, along with previous Auger and electron energy loss spectroscopic results [54, 55] suggest that there may be a similar process on the surface as a result of electron radiation.

The irradiation-induced topological and compositional changes are certainly related to the problem of electron stimulated desorption, especially with the desorption of neutral atoms, the dominant component of the desorbed species. While it is generally agreed that the desorption processes started with the non-radiative recombination of the excitons, it is not clear how this localized excitation is mediated to the surface. One proposed mechanism that currently is considered favorably involves H center migration via a replacement-collision sequence along the (110) directions [75]. Halogen desorption occurs when this migration reaches the surface. While our work suggests that, as a result of electron bombardment, significant compositional changes can occur on the alkali halide surface, there may not be a perfect crystal lattice left for this type of migration except for the initial stage of damage. In any case, the aggregation of the alkali atoms has to be considered as a competing process.

ESD Studied By Mass Spectroscopy And Optical Spectroscopy

Electron-stimulated-desorption from KCl and NaCl single crystals and a KCl-NaCl mixed crystal were studied. The optical method was used to detect the desorbed neutral atoms that were in excited states, while the mass spectrometric method measured all neutral atoms, both in the ground and excited states. Since the excited-state neutrals constitute only a small portion of the total signal [76], we will refer to the mass-spectrometric signal as the ground-state desorption signal.

One of the advantages of the mass-spectrometric detection system is that all neutral species can be detected easily, while the laser-induced fluorescence (LIF) methods are limited to the detection of alkali atoms. We measured the dependence of desorption yields of both alkali and halogen neutrals on electron current. Figure 13 shows the data from the NaCl crystal sample with the electron current changed by a factor of 20. This dependence is shown to be linear. To minimize the effect of electron beam damage, each point was measured after annealing the sample at 350°C for an hour. Since the delay time of desorption is of the order of a millisecond, much shorter than the integration time for our experiment (a few seconds), this linear dependence does not necessarily indicate a direct process, rather it may only reflect the linear dependence of the rate of defect production or energy deposition on the incident electron current.

Figure 14 and Fig. 15 show the time dependence of the desorption yields, with continuing electron irradiation, of both the excited-state neutral alkali metal atoms and the ground state neutrals. The ground-

Figure 13. Electron current dependence of desorption yield from NaCl.

(.) Na, (+) Cl

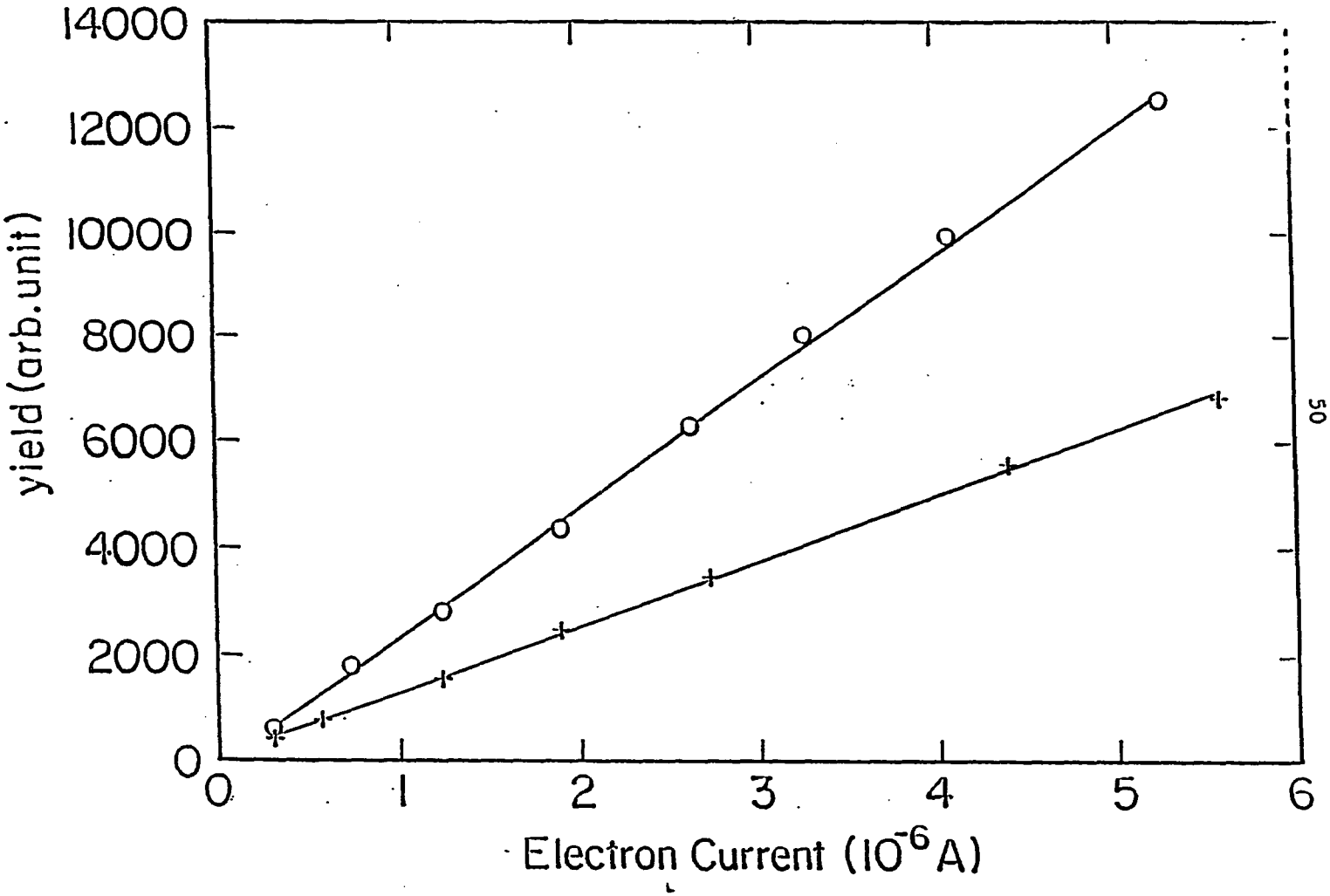
14000
12000
10000
8000
6000
4000
2000
0
yield (arb. unit)
0
1
2
3
4
5
6
Electron Current (10^{-6} A)
50

Figure 14. Time dependence of ground state desorption yields from NaCl.

(+), (.): Na and Cl at 205°C.

(x), (*): Na and Cl at 141°C

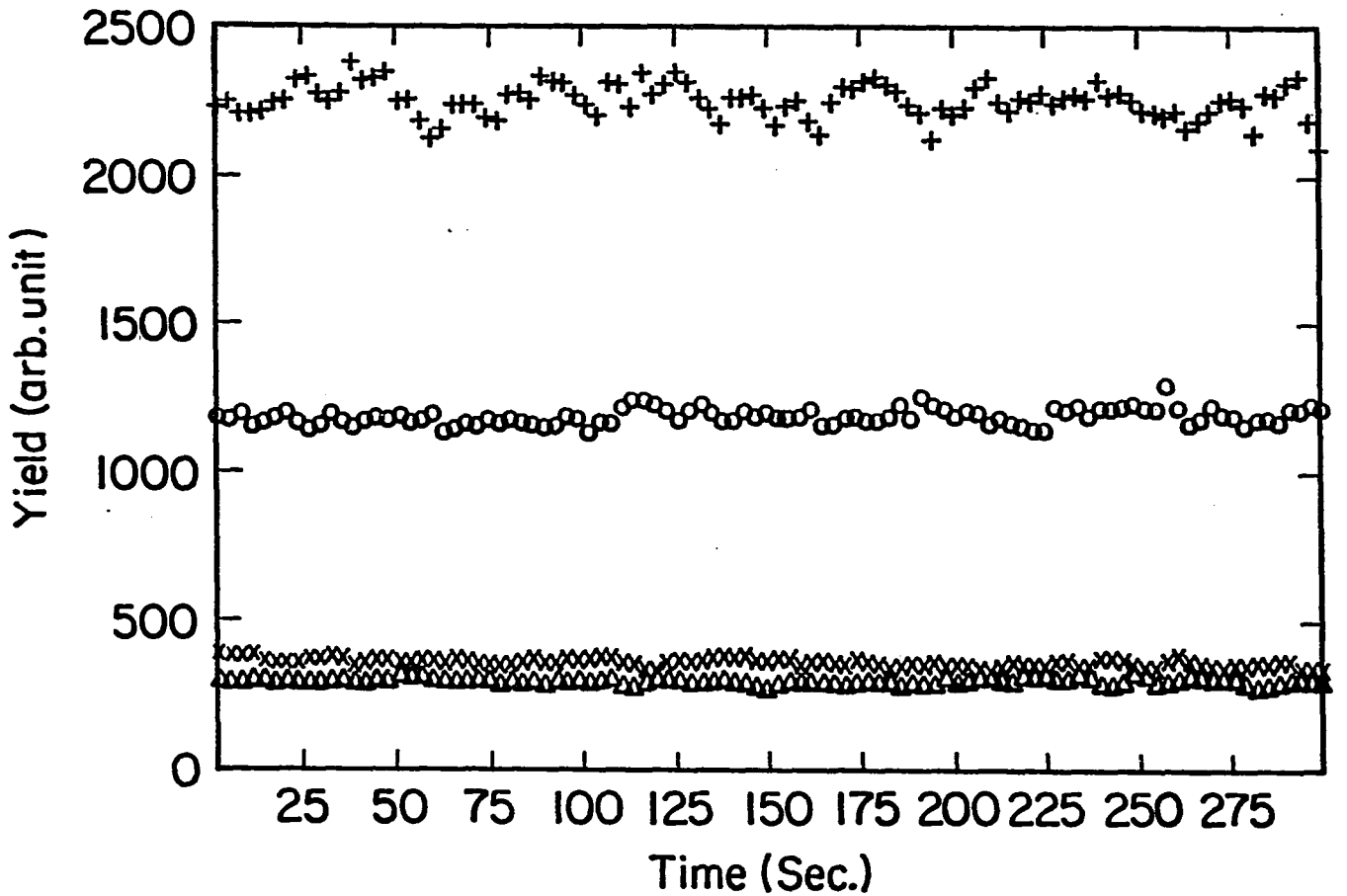
2500
2000
1500
1000
500
0
Yield (arb.unit)
25 50 75 100 125 150 175 200 225 250 275
Time (Sec.)

Figure 15. Time dependence of excited state Na desorption yield from NaCl at different temperatures.
(+) 205°C, (.) 141°C. The data are normalized at t=0.

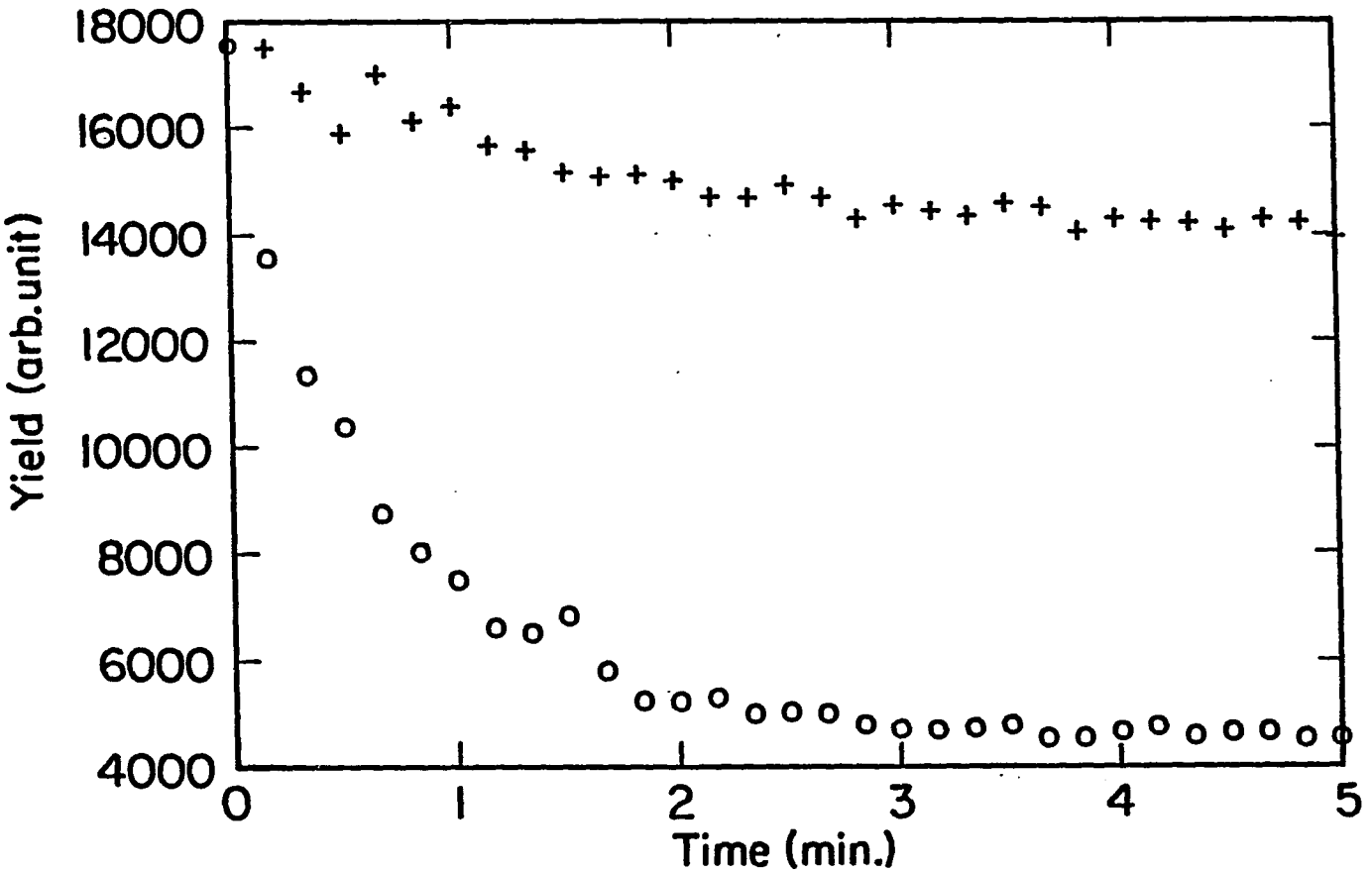
18000
16000
14000
12000
10000
8000
6000
4000
Yield (arb.unit)
0
1
2
3
4
5
Time (min.)

state spectra showed little time dependence. This shows that the ground state neutral is not sensitive to the surface conditions. This is in general agreement with the indirect model. This lack of time dependence, together with our previous observations on the changes of the surfaces upon electron irradiation, shows that neutral atom ESD from alkali halides is not a suitable candidate for surface spectroscopy. On the other hand, the excited state neutral atom desorption showed a strong temperature dependent decay. This does not necessarily contradict the proposal of Walkup et al. [38] that the excited state neutrals are produced by secondary electrons exciting the desorbed ground state neutral, since it is reasonable to expect the number of secondary electrons to decrease when the surface becomes metallized, due to its smaller mean free path compared with that of the insulators. However, the time dependence we have measured does show the difficulty of measuring the electron current dependence of the yield, which is one of the most important supporting behaviors for the secondary-electron mechanism.

The temperature dependence of the ground-state neutral desorption yields were measured. Figure 16 and Fig 17 show the yields of alkali metal atoms and Cl atoms vs. the reciprocal temperature. (Because of the different ionization probability for alkali and halide in the RGA, the yields can not be compared directly.) These data are in general agreement with previous results. The ratio of the yields of alkali and halide atoms is basically independent of temperature, and the yields of each increase with increasing temperature. We can see that the temperature dependence can be divided into two linear regions, each

Figure 16. Temperature dependence of ground state neutral desorption yields from NaCl and the vapor pressure of Na.
(+) Na, (*) Cl.

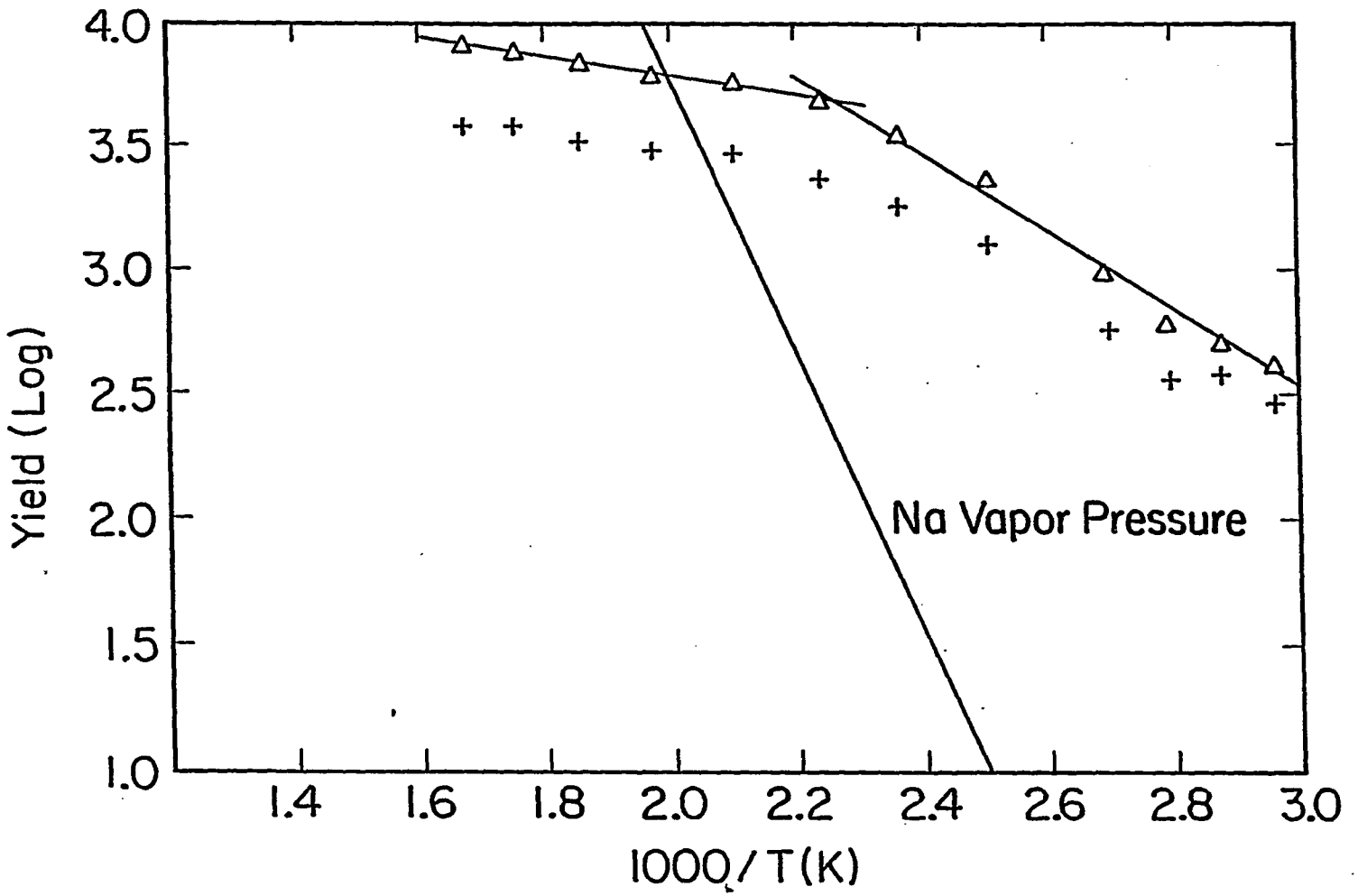
4.0
3.5
3.0
2.5
2.0
1.5
1.0
Yield (Log)
1.4
1.6
1.8
2.0
2.2
2.4
2.6
2.8
3.0
1000/T(K)
Na Vapor Pressure

Figure 17. Temperature dependence of ground state neutral desorption yields from KCl and the vapor pressure of K.
(△) K, (+) Cl.

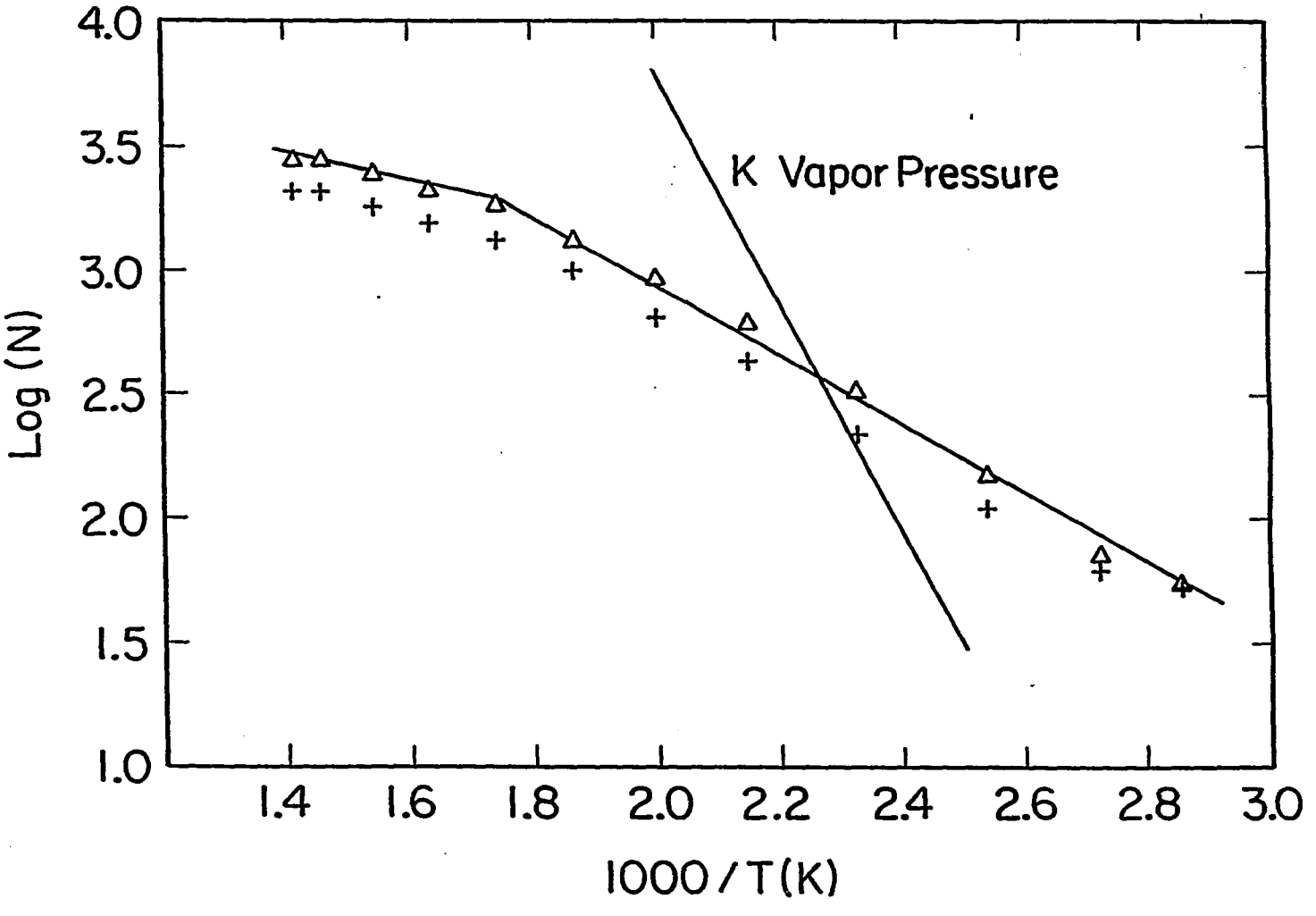
4.0
3.5
3.0
2.5
2.0
1.5
1.0
Log (N)
K Vapor Pressure
1.4
1.6
1.8
2.0
2.2
2.4
2.6
2.8
3.0
1000 / T(K)

features a different activation energy (slope), i.e.,

$$Y = C \exp(-E/kT)$$

where Y is the yield, k the Boltzmann constant and E the activation energy. In the lower temperature regions the activation energy is higher (see Table 2). Since many have assumed that the alkali metal desorption resulted from thermal evaporation of excess metal atoms, we have also included in the graphs curves showing the vapor pressure of the corresponding alkali metals in the same temperature range. They clearly do not match. To further test the relationship between desorption yield and vapor pressure, we grew mixed crystals of KCl and NaCl. They are known to form solid solutions at all compositions and assume the NaCl structure with lattice that constants change continuously from that of one crystal to the other [77]. Figure 18 shows the ratio of the yields of K and Na from the KCl-NaCl mixed crystal sample, as well as the ratio of the vapor pressures of the two alkalis. There is also no correlation. This shows that the desorption yield is not simply proportional to the vapor pressure.

The increase of desorption yields with temperature can be understood in terms of either an increased evaporation rate or a thermally activated defect migration process, as proposed by Loubriel et al. [53], for example. It is clear that the measured activation energies are much lower than those of the thermal evaporation. These data indicate that the thermal evaporation can not be the rate-limiting process in the desorption.

Using a transmission electron microscope, Hobbs [27] showed that the

efficiency of colloid production by electron irradiation in NaCl reaches a maximum at 150°C, about the same temperature at which we observed the change of slope in the desorption yield, and then decreases with increasing temperature. No colloids were observed above 230°C. This, together with our previous observation in the SEM, suggests that at low temperatures (from room temperature up to 150°C), desorption is strongly coupled with the process of colloid formation. But at higher temperatures, the desorption is governed by a different process.

Many experiments have shown that in about the same temperature range as in our study, the F center production rate decreases sharply with increasing temperature [78, 79], possibly due to the increased vacancy mobility and consequently the annihilation of electrons and holes at impurity recombination centers with no defect production [80]. This effect, we notice, can offer a qualitative explanation for the slowing down of the desorption rate.

These data indicate that a transition temperature exists (160°C for NaCl and 280°C for KCl). The ESD process is quite different above and below this temperature. The lower temperature case should be connected to the large scale topological and compositional changes we presented earlier. A complete theory of ESD should take this into account and explain or describe

1). The state of the surface under irradiation and how it changes with temperature.

2). Temperature dependence of the yields

3). Kinetic energy distributions, especially the non-thermal part.

Figure 18. Temperature dependence of the ratio of the desorption yields between K and Na from a KCl-NaCl mixed crystal and the ratio of the two vapor pressures.

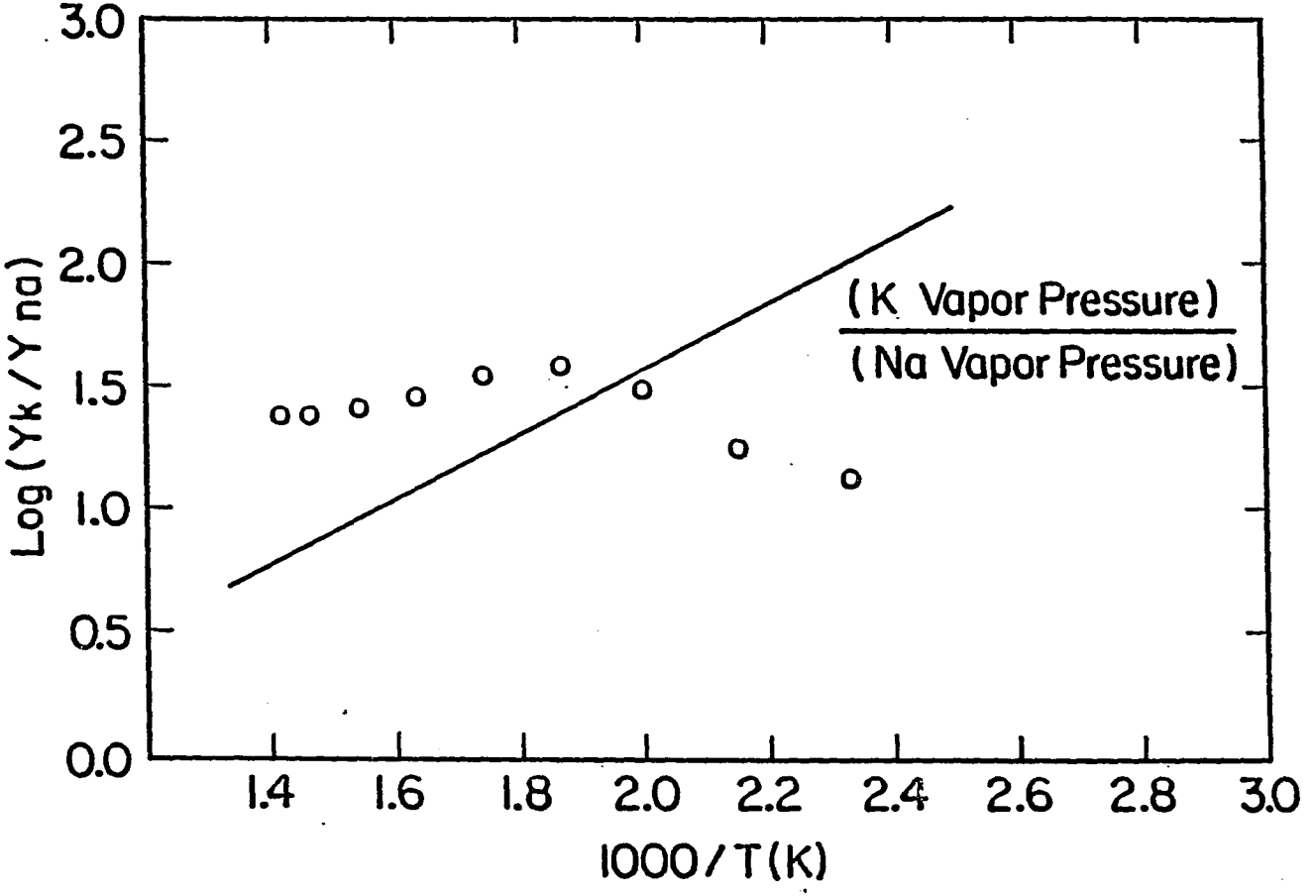
3.0
2.5
2.0
1.5
1.0
0.5
0.0
Log (Yk / Yna)
1.4
1.6
1.8
2.0
2.2
2.4
2.6
2.8
3.0
1000 / T(K)
(K Vapor Pressure)
(Na Vapor Pressure)

Table 2. Activation energies of the ESD processes and thermal evaporations

	NaCl	KCl
activation energy of neutral desorption (eV)		
region 1 (low temperature)	0.29	0.27
region 2 (high temperature)	0.073	0.12
activation energy of thermal evaporation	1.07	0.88

4). The passage of energy transfer to the surface, when it is metallized.

5). The apparent contradiction between the large scale-change on the surface and the lack of change of the ground state yields.

Electron Irradiation Induced Decomposition Of CaF_2 Thin Films

CaF_2 is considered a technologically important material because high quality CaF_2 films can be grown epitaxially on Si(111), making CaF_2/Si a model system for studying insulator and semiconductor epitaxial structure, which is of great importance to the integrated circuit industry [81, 82]. CaF_2 and other crystals with the fluorite structure are also very similar to alkali halides in that they are all strongly ionic insulators and color centers with similar structures (F, V_k and H centers, for example) can be generated in both systems [83, 84, 85]. For these reasons we have chosen CaF_2 to extend our study of electron beam interaction with ionic insulators.

Previous studies on electron beam interaction with CaF_2 exist. Betz et al. [86] observed no Ca desorption upon electron bombardment at low temperatures (< 500 K), and this is probably due to the lower vapor pressure of Ca. Strecher et al. [87] studied electron beam decomposition of CaF_2 surface cleaned by ion beam bombardment. They observed the loss of F atoms from the surface as evidenced by the decrease of the F Auger intensity. They have also observed the splitting of the Ca 2p level in photoemission, which they attributed to the change of coordination number and the oxidation of the surface Ca atoms. Carlsson et al. [88]

studied ultraviolet irradiation induced effects on the CaF_2/Si system (with film thickness about 10 Å) using angle resolved photoemission and concluded that a new ordered structure was formed on the surface.

We used AES, SEM, SAM and EDX to study electron-induced structure changes and decomposition, especially its temperature dependence, on a CaF_2 surface. The setup is the same as in the previous experiment, but 7 keV electrons were used since we observed smaller charging effects with this primary energy. The thin film CaF_2 sample, with a thickness of about 2500 Å, was prepared in the same way as the alkali halide films in the previous studies. The impurity content of the powders used for evaporation is listed in Table 3 but the thin film sample was not chemically analyzed. It is known that the efficiency of defect production is very low in pure CaF_2 and the presence of impurities can greatly increase the efficiency. With each different temperature, the measurements were taken at a fresh area of the sample surface.

Figure 19 is an Auger spectrum of the CaF_2 sample. It shows no oxygen and sulfur contamination and very little carbon. Figure 20 is an Energy-Dispersive-X-ray (EDX) spectrum. The appearance of the substrate Ni peak indicates that the 7 KeV electron can penetrate the whole film. Thus while the Auger spectrum measures the surface composition, the F EDX signal give us a measure of the bulk concentration of these atoms.

Similar electron radiation-induced changes in the SEM micrograph as with the alkali halides were observed (Fig. 21). The film changes from very smooth and uniform to non-uniform and some bright spots appear. However, there are differences between these two systems in that with

Table 3. Impurity content of the CaF_2 powder used for evaporation

Cl	0.01%
NH3	0.002%
SO4	0.01%
Fe	0.001%
Ba	0.01%
Heavy metals (Pb, etc)	0.003%

Figure 19. Auger spectrum of CaF_2.

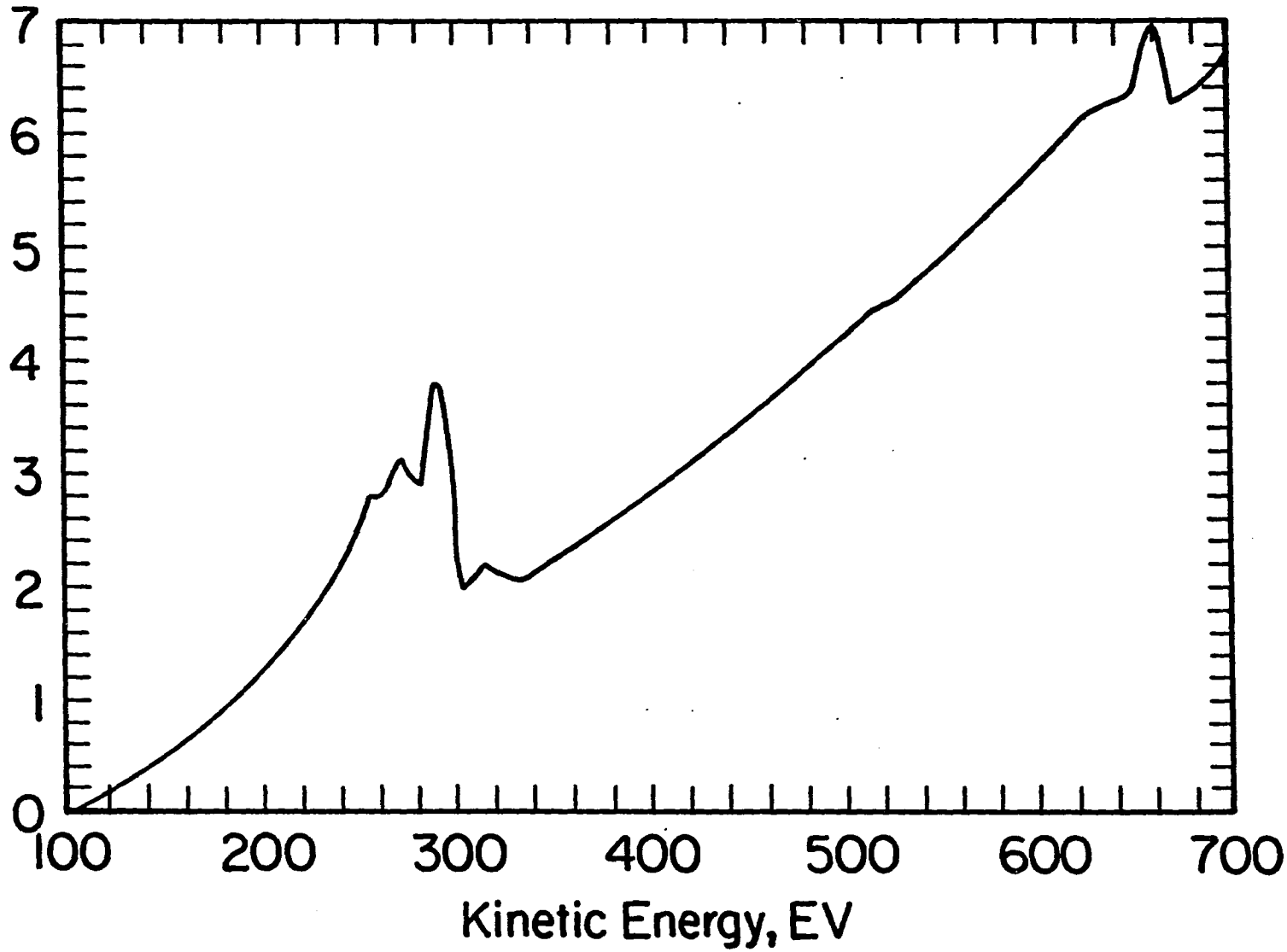
7
6
5
4
3
2
1
0
100
200
300
400
500
600
700
Kinetic Energy, EV

Figure 20. EDX spectrum of CaF_2 thin film on Ni substrate.

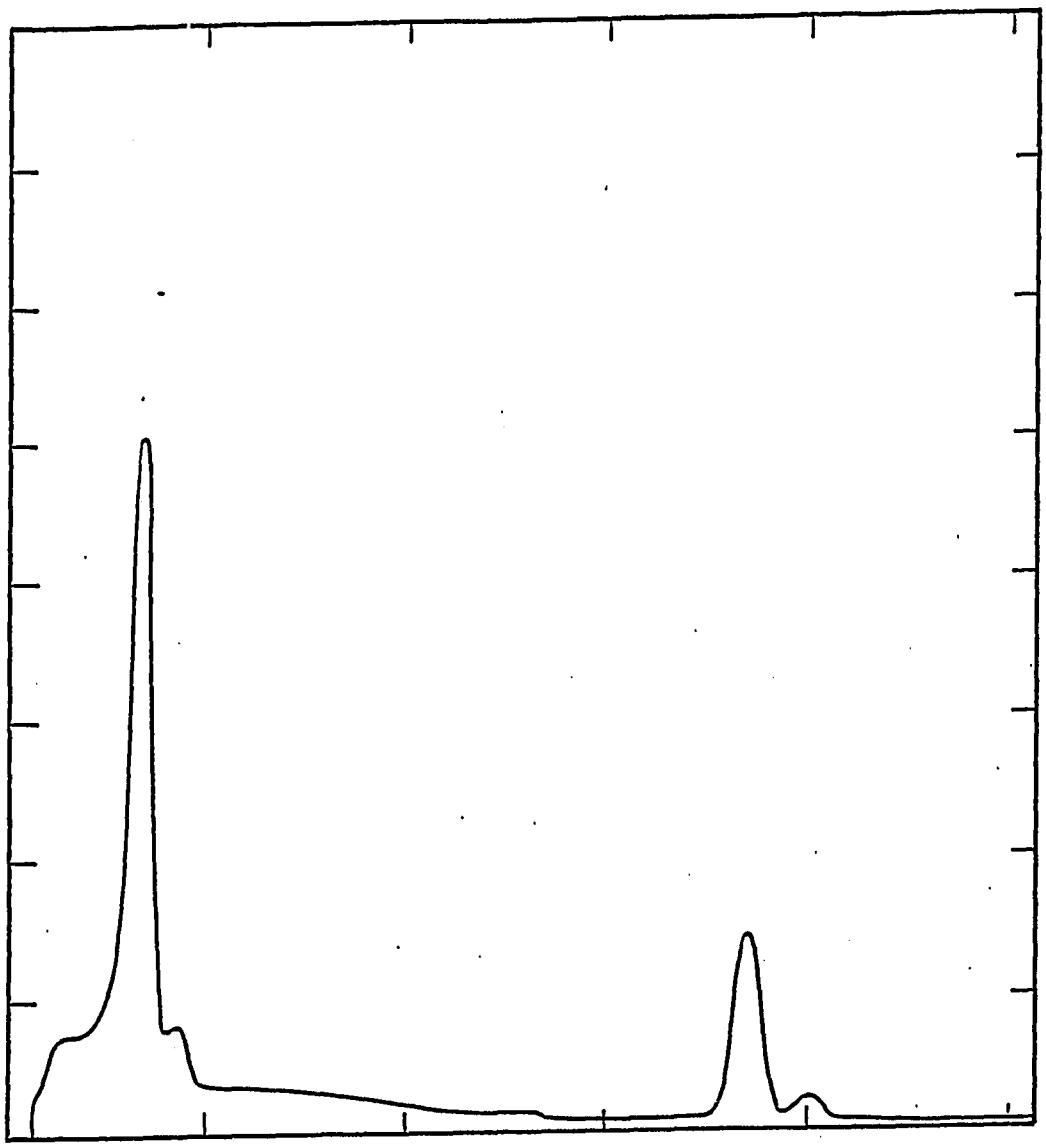

0

5.12

KINETIC ENERGY (KEV)

Figure 21: SEM micrograph of CaF_2 at 5000x.

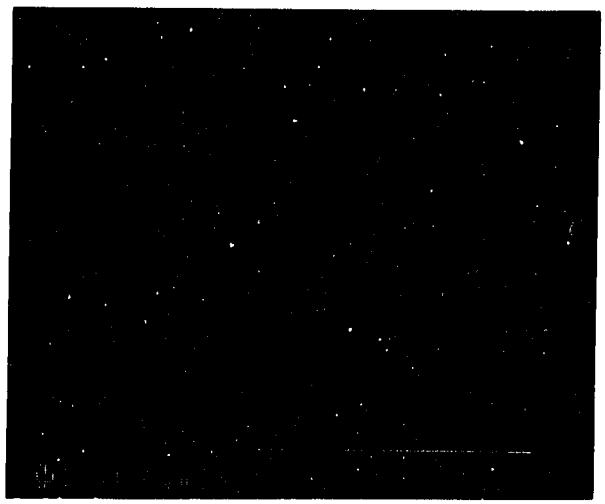

CaF_2 these features disappear with further electron radiation and it is not clear whether they are correlated with topological changes. Because of their transient nature, we were not able to take any scanning Auger micrographs. But by analogy with features in the alkali halide samples we would expect that they correspond to different compositions.

Figure 22 and Fig. 23 are low-energy Auger spectra and their second derivatives for CaF_2 with Fig. 20a taken at a fresh area of the sample while Fig. 20b was taken at an area that has undergone some electron irradiation (about 10 nA for 10 min). From Fig. 24, one can see that two new peaks appear in the spectrum taken at the damaged area. These two peaks correspond to transitions between valence electrons and the Ca 3p band, i.e., an intra-atomic process. In an undamaged CaF_2 crystal, the valence electrons are well localized on the F site, thus making the probability of Ca MVV Auger transition involving these electrons vanishingly small. After some F desorbed from the surface, and the nearby Ca ions were reduced, we were able to detect this transition. This effect is shown more clearly with a MgF_2 thin film sample similarly prepared (see Fig. 24) since in this case the Auger peak energy is higher and is easier to distinguish from the secondary electron background. Since the cation Auger transition involving valence electrons increases from zero in an undamaged ionic crystal to a large value in a damaged one, we propose that this Auger transition can be used as a sensitive gauge of radiation-induced damage on the surface of ionic crystals.

Figure 25 shows the measured dependence of the F KVV Auger signal

Figure 22. Low energy Auger spectra of CaF_2. A). Undamaged sample. B). Damaged sample.

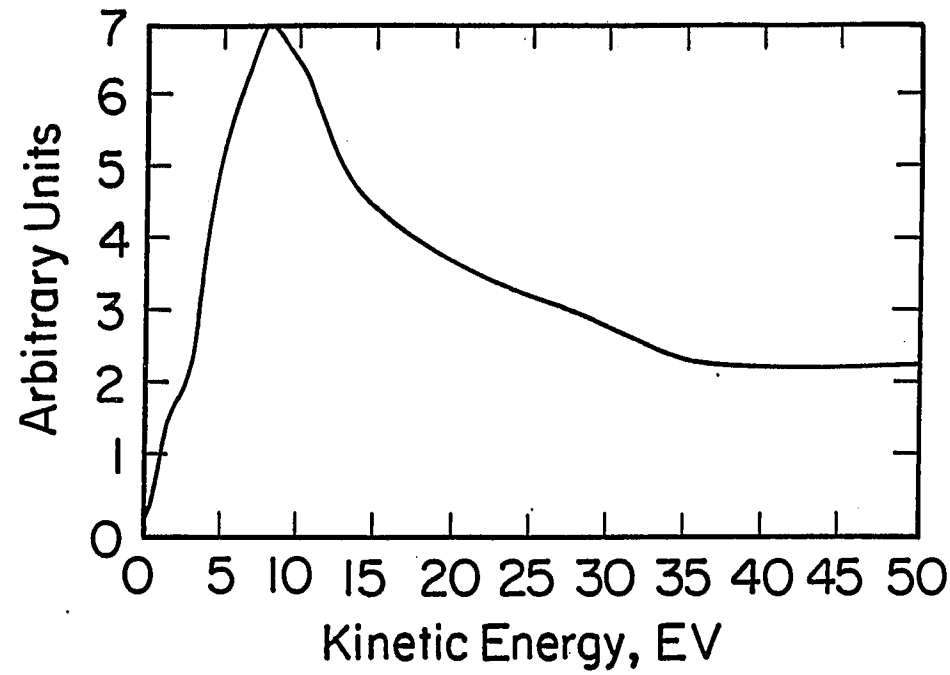
Arbitrary Units
0
1
2
3
4
5
6
7
0 5 10 15 20 25 30 35 40 45 50
Kinetic Energy, EV

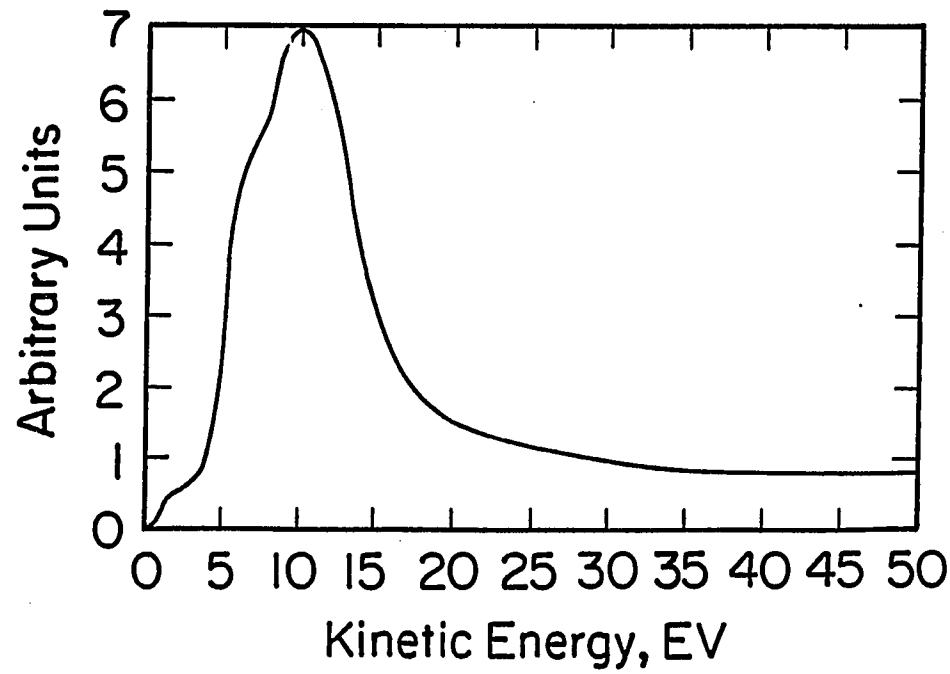
Arbitrary Units
0
1
2
3
4
5
6
7
0 5 10 15 20 25 30 35 40 45 50
Kinetic Energy, EV

Figure 23. Second derivatives of the spectra in Fig. 22.

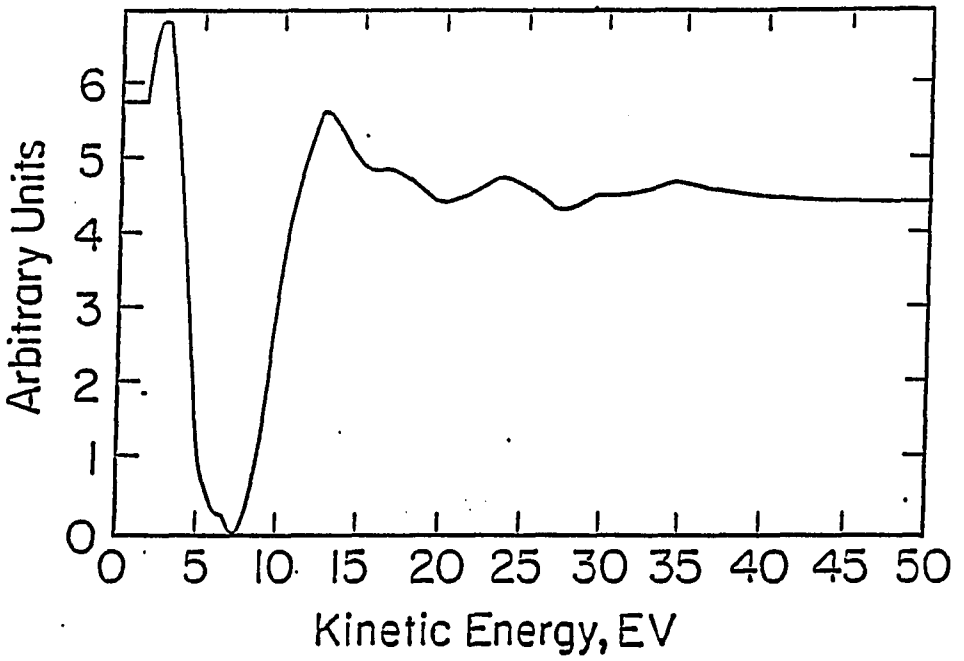
Arbitrary Units
0
1
2
3
4
5
6
0 5 10 15 20 25 30 35 40 45 50
Kinetic Energy, EV

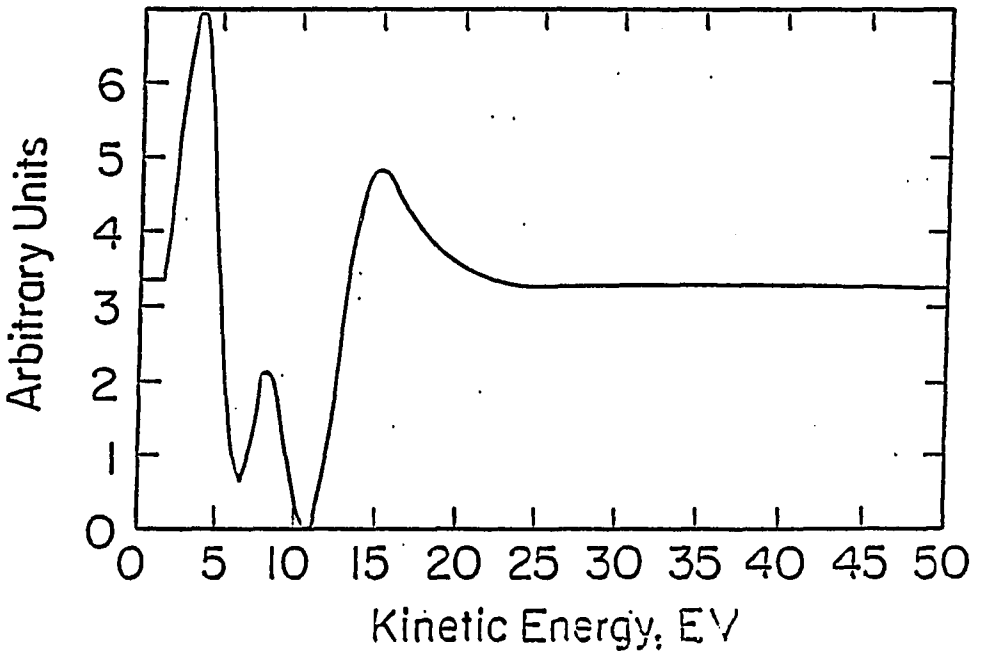
Arbitrary Units
0
1
2
3
4
5
6
0 5 10 15 20 25 30 35 40 45 50
Kinetic Energy, EV

Figure 24. Low energy Auger spectra of MgF_2. A). Undamaged sample. B). Damaged sample.

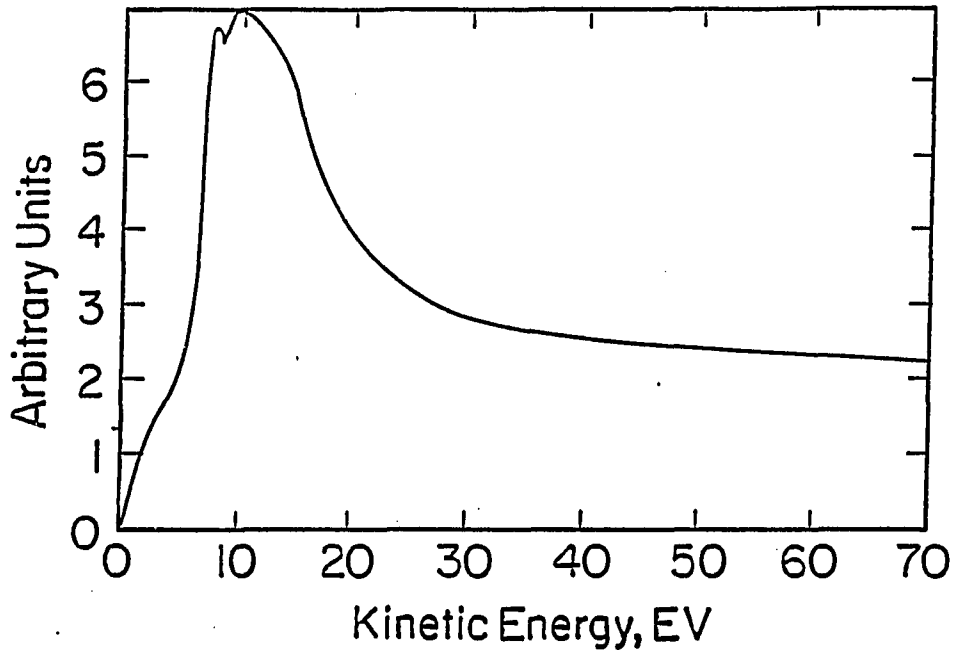
Arbitrary Units
0
1
2
3
4
5
6
0
10
20
30
40
50
60
70
Kinetic Energy, EV

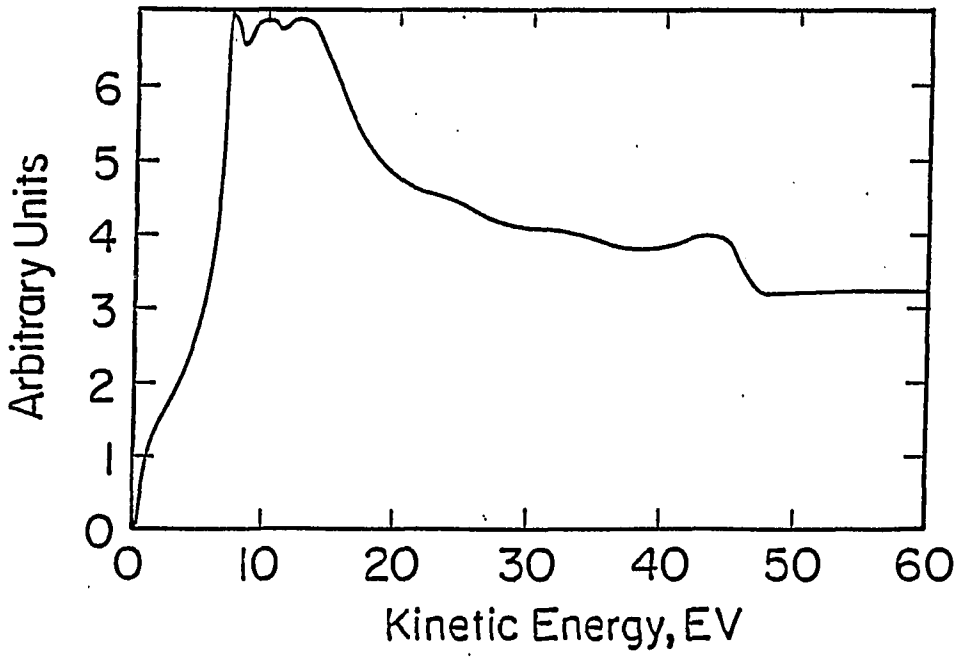
Arbitrary Units
0
1
2
3
4
5
6
0
10
20
30
40
50
60
Kinetic Energy, EV

Figure 25. F KVV Auger (661 eV) time dependence at different temperatures. + 90°C, x 135°C, * 170°C, o 210°C. Oxygen Auger at 170°C is also shown.

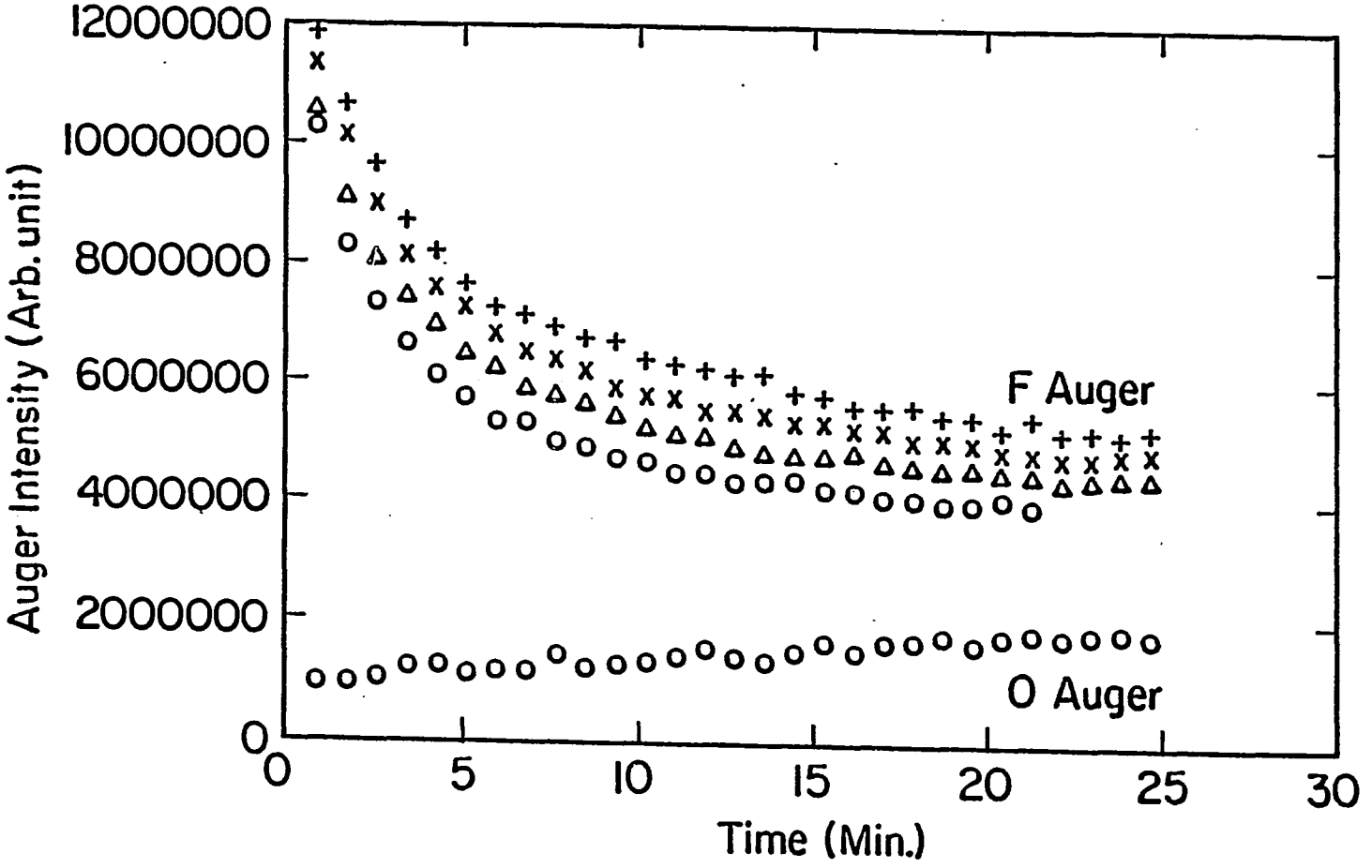
12000000
10000000
8000000
6000000
4000000
2000000
0
Auger Intensity (Arb. unit)
0
5
10
15
20
25
30
Time (Min.)
F Auger
O Auger

(661 eV) with electron radiation dose at four different temperatures. The O2 peak at 512 eV was observed to increase slightly, due to the oxidation of the free Ca atoms on the surface, but it was still very small compared to that of either Ca or F. The F Auger signal is a measure of the F surface coverage, and it is shown to be decreasing rapidly when irradiated by electrons, indicating loss of F atoms. This is similar to the result of Strecher et al. [87]. The data also show that this decrease does not feature any temperature dependence, so the rate of desorption from the surface is a function of F surface coverage only.

The decrease of the EDX F peak with increasing radiation (Fig. 26), however, showed a strong temperature dependence, with faster decay at higher temperature. The data can be fitted very well to:

$$F(t) = A \exp(-B\ t) + C$$

where F(t) is the peak height of the F EDX signal, and A, B, and C are constants. (See table 4 for the fitted data.) Thus the desorption rate should be:

$$R = -dF/dt = A\ B \exp(-B \times t)$$

Since B is basically independent of temperature, when A is plotted against 1/T(K) (Fig. 27), it falls on a straight line and gives a well defined activation energy of 0.15 eV for the bulk desorption process.

Figure 26. F EDX signal time dependence at different temperatures. The curves are least square fit to the exponential function.

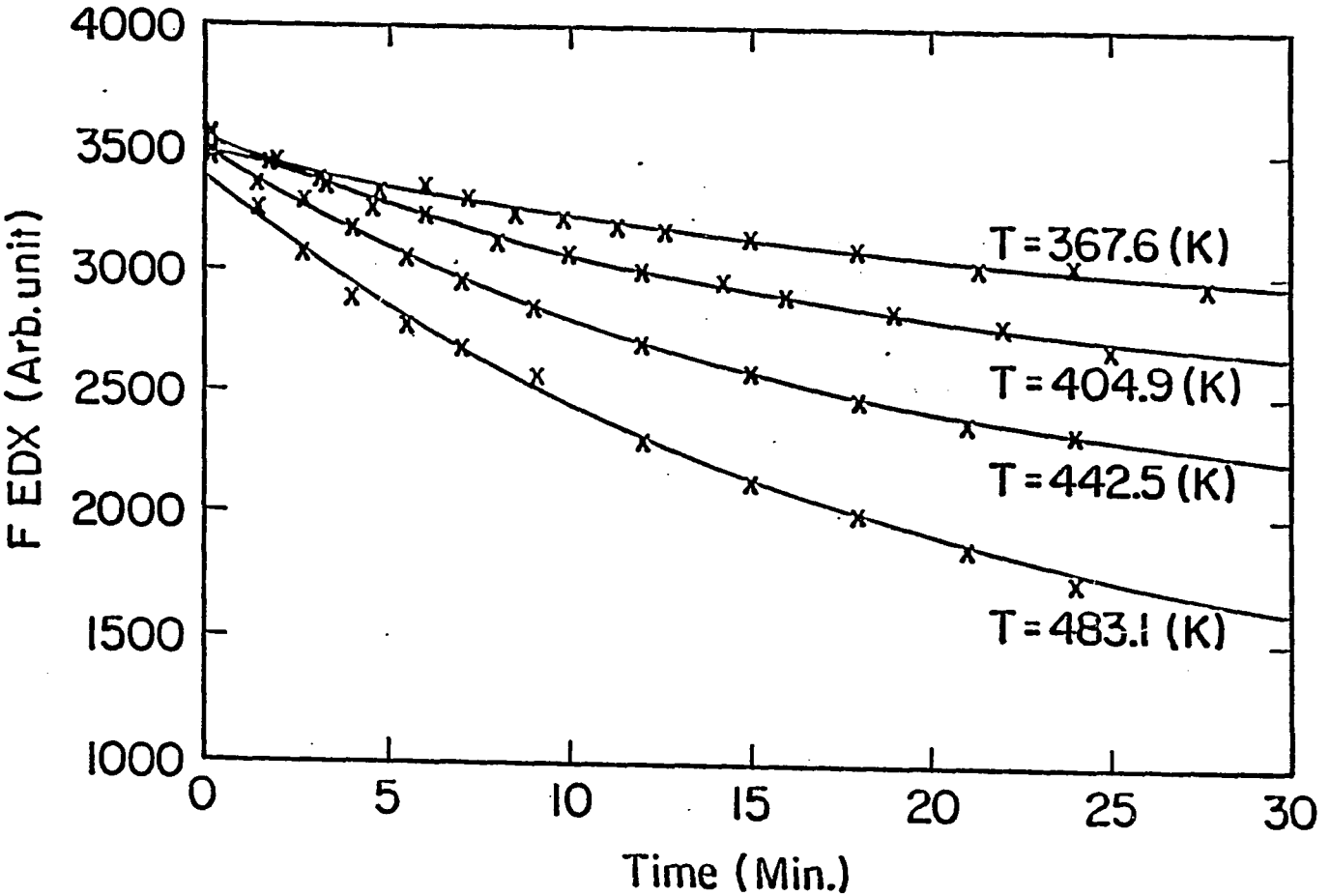
4000
3500
3000
2500
2000
1500
1000
F EDX (Arb.unit)
0
5
10
15
20
25
30
Time (Min.)
T=367.6 (K)
T=404.9 (K)
T=442.5 (K)
T=483.1 (K)

Table 4. Fit EDX time dependence.

Temperature(K)	1000/T(K)	A	C	B(min.$^{-1}$)
483.1	2.07	2160.6	1214.5	0.056
442.5	2.26	1483.9	2009.1	0.060
404.9	2.47	1067.6	2461.0	0.056
367.6	2.72	709.2	2770.2	0.057

Figure 27. A vs. 1000/T (K)

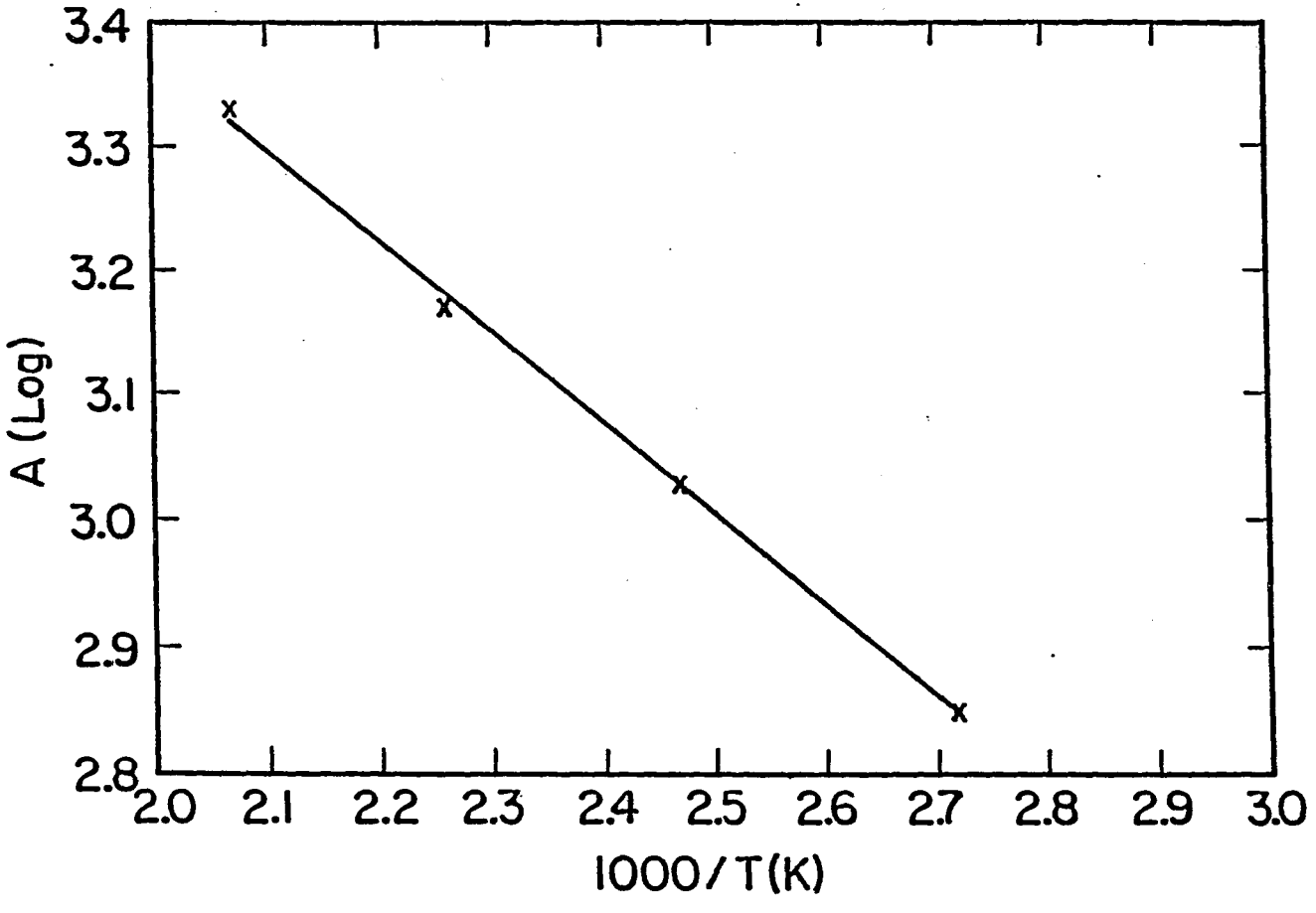
3.4
3.3
3.2
3.1
3.0
2.9
2.8
A (Log)
2.0
2.1
2.2
2.3
2.4
2.5
2.6
2.7
2.8
2.9
3.0
1000/T(K)

This indicates that the desorption process is rate limited by a diffusion process.

CONCLUSIONS

The interaction of low energy electron beams with alkali halides and CaF_2 were studied using mass-spectroscopy and scanning-electron microscopy. It was observed that the electron beam caused the sample surfaces to be metal rich. Metal clusters of sizes up to 2 m were formed on the surfaces. The temperature dependence of desorption yields as studied by mass spectroscopy show two different activation energy at two temperature regions. This transition temperature may be related to the formation of clusters. The desorption yield was found to be not sensitive to the surface conditions, thus the desorption phenomenon is not suitable as a surface spectroscopy. It was observed that the desorption process in CaF_2 is governed by diffusion and is characterized by a single activation energy. It was also observed that the Auger transitions involving valence electrons are very sensitive to surface damage and can be used as a gauge of the damage.

REFERENCES

1. P. W. Palmberg and T. N. Rhodin, J. Phys. Chem. Solids 29, 1917 (1968)
2. P. D. Townsend and J. C. Kelly, Phys. Lett. 26A, 138 (1968)
3. N. H. Tolk, M. M. Traum, J. C. Tully, and T. E. Madey, eds. "Desorption Induced by Electronic Transitions - DIET I" (Springer, Berlin, 1983).
4. W. Brenig and D. Menzel, eds. "Desorption Induced by Electronic Transitions - DIET II" (Springer, Berlin, 1985).
5. C. G. Pantano and T. E. Madey, Appl. Surf. Sci. 7, 115 (1981)
6. H. Yokoyama, Appl. Phys. Lett. 49, 20 (1986)
7. J. Block, N. Shamia and Y. Zeiri, Appl. Phys. Lett. 52, 14 (1988)
8. D. Pooley, Solid State Commun. 3, 241 (1965)
9. D. Pooley, Proc. Phys. Soc. 81, 245 (1966)
10. N. H. Hersh, Phys. Rev. 148, 928 (1966)
11. R. B. Murray and F.J. Keller, Phys. Rev. A, 153, 993 (1967)
12. R. B. Murray and F.J. Keller, Phys. Rev. A, 137, 942 (1965)
13. M. N. Kabler, Phys. Rev., 136, 1296 (1964)
14. C. C. Klick and J. H. Schulman, Solid State Physics, Vol. 5, eds. F. Seitz and D. Turnbull (Academic Press, New York, 1956)
15. J. H. O. Varley, J. Nucl. Energy, 1, 130 (1954)
16. F. E. Williams, Phys. Rev. 126, 70 (1962)
17. C. C. Klick, Phys. Rev. 120, 760 (1960)
18. J. Sharma and R. Smoluchowski, Phys. Rev. A 137, 259 (1965)

19. F. C. Brown, B. R. Sever and J. P. Scott, Phys. Rev. Lett. 57, 2279 (1986)

20. T. Karasawa, M. Hirai, J. Phys. Soc. Japan, 34, 276 (1973)

21. I. N. Bradford, R. T. Williams, W. L. Faust, Phys. Lett. 35, 300 (1975)

22. T. Karasawa, M. Hirai, J. Phys. Soc. Japan, 33, 1728 (1972)

23. A. M. Stoneham, Theory of Defects in Solids (University Press, Oxford, 1975)

24. K. Shvarts, Y. A. Ekmanis, V. V. Udod, A. F. Lyushina, Y. E. Tiliks and R. A. Kan, Sov. Phys. Solid State 12, 679 (1970)

25. U. Jain and A. B. Lidiard, Phil. Mag. 35, 245 (1977)

26. L.W. Hobbs, A.E. Hughes, and G. Chassagne, Nature 252, 383 (1974)

27. L. W. Hobbs in Surface and Defect Properties of Solids (American Chemical Society Specialist Periodical Reports), Vol. 4, 171 (1975)

28. P. E. Readhead, Can. J. Phys. 42, 886 (1964)

29. D. Menzel and R. Gomer, J. Chem. Phys. 41, 3311 (1964)

30. T. E. Madey and J. T. Yates, Jr., Surf. Sci. 63,203 (1977)

31. D. Menzel, Nucl. Instru. Meth. Phys. Res. B13, 507 (1986)

32. R. Treichler, W. Riedl, W. Wurth, P. Feulner and D. Menzel, Phys. Rev. Lett. 54, 462 (1985)

33. H. Niehus, Appl. Surf. Sci. 13, 292 (1982)

34. W. Riedl and D. Menzel, Surf. Sci. 163, 39 (1985)

35. N. H. Tolk, M. M. Traum, J. S. Kraus, T. R. Pian and W. E. Collins, Phys. Rev. Lett. 49, 812 (1982)

36. N. H. Tolk, L. C. Feldman, J. S. Kraus, R. J. Morris, M. M. Traum, and J. C. Tully, Phys. Rev. Lett. 46, 134 (1981)

37. T. R. Pian, N. R. Tolk, M. M. Traum, and J. Kraus, Surf. Sci. 129, 573 (1983).

38. R. E. Walkup, Ph. Avouris, and A. P. Ghosh, Phys. Rev. Lett 57, 2227 (1986).

39. R. E. Walkup, Ph. Avouris, and A. P. Ghosh, Phys. Rev. B36, 4577 (1987)

40. N. G. Stoffel, R. Riedel, E. Colavita, G. Margaritondo, R. F. Haglund, Jr., E. Taglauer and N. H. Tolk, Phys. Rev. 32, 6805 (1985)

41. C. C. Parks, Z. Hussain, D. A. Shirley, M. L. Knotek, G. Loubriel, and R. A. Rosenberg, Phys. Rev. B 28, 4793 (1983)

42. R. F. Haglund Jr, R. G. Albridge, D. W. Cherry, R. K. Cole, M. H. Mendenhall, W. C. B. Peatman and N. H. Tolk, Nucl. Instru. Meth. Phys. Res. B13, 525 (1986)

43. T. R. Pian, M. M. Traum, J. S. Kraus, N. H. Tolk, N. G. Stoffel and G. Magaritondo, Surf. Sci. 128, 13 (1983)

44. T. Yasue and A. Ichimiya, Surf. Sci. 186, 191 (1987)

45. R. F. Haglund, Jr., P. G. Albridge, D. W. Cherry, R. K. Cole, M. H. Mendenhall, W. C. B. Peatman and N. H. Tolk, Nucl. Instr. Meth. Phys. Res. B13, 525 (1986)

46. H. Overeijnder, M. Szymonski, A. Haring, A. E. de Vries, Rad. Effects 36, 63 (1978)

48. M. Szymonsky, H. Overeijnder and A. E. De Vries, Surf. Sci. 90, 274 (1979)

49. P. D. Townsend, R. Browning, D. J. Garlant, J. C. Kelly, A. Mahjoobi, A. J. Michael, and M. Saidoh, Rad. Eff. 30, 55 (1976).

50. Z. Postawa and M. Szymonski, Phys. Rev. B 39, 12950 (1989)

51. H. Overeijnder, R. R. Ritol and A. E. de Vries, Surf. Sci. 90, 265 (1979)

52. H. Kanzaki and T. Mori, Phys. Rev. B 29, 3573 (1984)

53. G. M. Loubriel, T. A. Green, P. M. Richard, R. G. Albridge, D. W. Cherry, R. K. Cole, R. F. Haglund, L. T. Hudson, M. H. Mendenhall, D. M. Newns, P. M. Savundararaj, K. J. Snowdon and N. H. Tolk, Phys. Rev. Lett. 57, 1781 (1986)

54. T. A. Green, G. M. Loubriel, P. M. Richards, N. H. Tolk and R. F. Haglund, Phys. Rev. B 35, 781 (1987)

55. D. G. Lord and T. E. Gallon, Surf. Sci. 36, 606 (1973).

56. G. C. Freyburg and R. A. Lad, Surf. Sci. 48, 353 (1975).

57. L. S. Cota Araiza and B. D. Powell, Surf. Sci. 51, 504 (1975).

58. G. Singh and T. E. Gallon, Solid State Commun. 51, 281 (1984).

59. T. E. Gallon, Surf. Sci. 206, 365 (1988).

60. M. L. Knotek, P. J. Feibelman, Phys. Rev. Lett. 40, 964 (1979)

61. P. J. Feibelman, M. L. Knotek, Phys. Rev. B 18, 6531 (1978)

62. M. L. Knotek, P. J. Feibelman, Surf. Sci. 90, 78 (1979)

63. M. L. Knotek, Phys. Today, P24, Sept. 1984.

64. M. Szymonsky, Radiat. Eff. 52, 9 (1980)

64. M. Szymonsky, Radiat. Eff. 52, 9 (1980)

65. F. Agullo-Lopez and P. D. Townsend, Phys. Status Solidi B 97, 265 (1979)

66. R. E. Walkup and Ph. Avouris, Phys. Rev. Lett. 56, 524 (1986)

67. P. W. Erdman, E. C. Zipf, Rev. of Sci. Instrum. 53, 225 (1982)

68. P. W. Erdman, Ph.D. Thesis, University of Pittsburgh, 1982

69. H. Rabin, C. C. Klick, Phys. Rev. 117, (1960)

70. J. Estel, H. Hoinkes, H. Kaarmann, H. Nahr, and H. Wilsch, Surf. Sci. 54, 393 (1976).

71. C. C. Parks, D. A. Shirley, and G. Loubriel, Phys. Rev. B29, 4709 (1984).

72. T. R. Pian, Ph.D. thesis, University of Wisconsin, 1982.

73. D. J. Elliott, P. D. Townsend, Philos. Mag. 23, 249(1971)

74. K. L. Tsang, C. H. Zhang, T. A. Callcott, E. T. Arakawa, and D. L. Ederer, Phys. Rev. B35, 8374 (1987).

75. P. D. Townsend in " Sputtering by Particle Bombardment II ", ed. R. Behrisch, P147 (Springer-Verlag, New York, 1983)

76. E. Taglauer, N. Tolk, R. Riedel, E. Colavita, G. Margaritondo, N. Gershenfeld, N. Stoffel, J. A. Kebler and G. Loubriel, Surf. Sci. 169, 267 (1986)

77. R. J. Gnaedinger, J. Phys. Chem. 21, 323 (1052)

78. R. O. Vilu, M. A. Elango, Sov. Phys. - Solid State, 7, 2967 (1966)

79. D. Comins and P. T. Wedepohl, Solid State Commun. 4, 537 (1966)

80. E. Sonder and W. A. Sibley in Point Defects in Solids, eds. J. H. Crawford and L. M. Slifkin (Plenum, New York, 1972)

81. J. F. Himpsel, U. O. Carlsson, J. F. Morar, D. Rieger and J. A. Yarmoff, Phys. Rev. Lett. 56, 1497 (1985)

82. T. P. Smith, III, J. M. Phillios, W. M. Augustyniak and P. J. Stiles, Appl. Phys. Lett. 45, 907 (1984)

83. J. Arends, Phys. Status Solidi 7, 805 (1964)

84. J. H. Beaumont, J. V. Gee and W. Hayes, J. Phys. C, 3, L152 (1970)

85. W. Hayes, ed. Crystals with the Fluorite Structure (Clarendon Press, Oxford, 1974)

86. G. Betz, E. Wolfrum, E. Wurz, K. Mader, B. Strehl, W. Hunsinsky, R. F. Haglund, Jr and N. H. Tolk in "Desorption Induced by Electronic Transitions - DIET III", R. H. Stulen and M. L. Knotek eds. (Springer, Berlin, 1988), p 278.

87. C. L. Strecher, W. E. Moddeman, J, T, Grant, J. Appl. Phys. 52, 6921 (1981)

88. U. O. Carlsson, F. J. Himpsel, J. F. Morar, F. R. McFeely, D. Rieger and J. A. Yarmoff, Phys. Rev. Lett. 57, 1247 (1986).